Electronic Supplementary Information

Synthesis and Properties of Hypervalent Electron-rich Pentacoordinate Nitrogen Compounds

Chenting Yan, [a] Masato Takeshita, [a] Jun-ya Nakatsuji, [a] Akihiro Kurosaki, [a] Kaoko Sato, [a] Rong Shang,*[a] Masaaki Nakamoto, [a] Yohsuke Yamamoto,*[a] Yohei Adachi,[b] Ko Furukawa, [c] Ryohei Kishi, [d] Masayoshi Nakano [d,e]

a. Department of Chemistry, Graduate School of Science, Hiroshima University, 1-3-1 Kagamiyama, Higashi-Hiroshima 739-8526, Japan
b. Department of Applied Chemistry, Graduate School of Engineering, Hiroshima University, 1-3-1 Kagamiyama, Higashi-Hiroshima 739-8526, Japan
c. Center for Coordination Research Facilities, Institute for Research Promotion, Niigata University, 8050 Ikarashi 2-no-cho, Nishi-ku, Niigata 950-2181, Japan
d. Department of Materials Engineering Science, Graduate School of Engineering Science, Osaka University, Toyonaka, Osaka 560-8531, Japan
e. Department of Materials Engineering Science, Graduate School of Engineering Science, Osaka University, Toyonaka, Osaka 560-8531, Japan

Contents

1. Experimental section

Experimental Procedures

Instrumentation and Chemicals

All manipulations were performed under Ar or N_2 atmosphere by using standard Schlenk or glove box techniques. All the solvents were dried prior to use. Column chromatography was carried out using Merck silica gel 60 and KANTO CHEMICAL silica gel 60N. The ^{1}H NMR (400 MHz), ^{13}C NMR (100 MHz) and ^{19}F NMR (376 MHz) spectra were recorded using a JEOL EX-400 spectrometers. The chemical shift (δ) are reported from the internal $CHCl_3$ for ^{1}H (δ 7.26) and from the internal $CDCl_3$ for ^{13}C (δ 77.0) and from the internal $CFCl_3$ for ^{19}F (δ 0.00). Mass spectra were recorded with a Thermo Fisher Scientific samples. The X-ray crystal structural analysis was performed using a Bruker APEX II Ultra. The DFT calculations were performed using the *Gaussian 16 program* package.

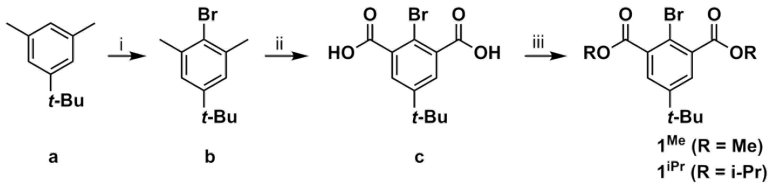

Scheme 1. Synthesis of methoxyl- and isopropoxyl-carbonyl substituted bromobenzenes. (i) Br_2, Fe, $CHCl_3$, room temperature (r.t.),3 h, 90%; (ii) $KMnO_4$, *t*-BuOH / H_2O, 95 ºC, 24 h, 97%; (iii) $\mathbf{1^{Me}}$, MeOH, H_2SO_4, 95 °C, 24 h, 82%; $\mathbf{1^{iPr}}$, *i*-PrOH, H_2SO_4,95 °C, 24 h, 78%;

1.1 Synthesis of 2-Bromo-5-*tert*-butyl-1,3-dimethylbenzene (b)

In a 250 mL round-bottom flask equipped with a magnetic stir bar and an addition funnel were added 5-*tert*-butyl-*m*-xylene (91.0 mL, 480 mmol) and iron powder (1.00 g, 1.36 mmol) to 75 mL of chloroform. The solution was cooled to 0 °C. A solution of bromine (27.5 mL, 525 mmol) in 25 mL of solution of chloroform was added dropwise via the addition funnel. The reaction was stirred for 3 h at room temperature and then poured into a cold solution of dilute aqueous NaOH (~1 M). The mixture was separated, and the aqueous layer was washed several times with CH_2Cl_2. The combined organic layers were dried with $MgSO_4$, filtered, and concentrated to a clear oil, which became a white solid upon standing. The crude solid was recrystallized from ethanol to give 105 g (437 mmol, 90% yield) of the title compound. ^{1}H NMR (400 MHz, $CDCl_3$) δ (ppm) 7.11 (s, 2H), 2.43 (s, 6H), 1.31 (s, 9H). ^{13}C NMR (100 MHz, $CDCl_3$) δ (ppm) 149.8, 137.8, 125.6, 124.6, 34.3, 31.4, 24.2. MS (GC-EI): $[M]^+$ $C_{12}H_{17}Br$ Calcd for: 240.05136 Found: 240.05148. M.P.: 48.5-49.8 °C.

1.2 Synthesis of 2-Bromo-5-*tert*-butyl-isophthalic Acid (c)

In a 500 mL three-necked round-bottom flask equipped with a mechanical stirrer and a reflux condenser was added 2-bromo-5-*tert*-butyl-1,3-dimethylbenzene (24.5 g, 101 mmol) and $KMnO_4$ (33.7 g, 214 mmol), dispersed in 200 mL of a 1:1 mixture of *tert*-butyl alcohol and water. The reaction mixture was heated to reflux for 1 h. After the mixture was cooled to room temperature, more $KMnO_4$ (33.2 g, 210 mmol) was added and the reaction mixture was refluxed for an additional 20 h. After the mixture was cooled to room temperature, the reaction was filtered through Celite and the filtrate was reduced by 1/3. The solution was acidified with concentrated HCl. The resulting white precipitate was collected by filteration and dissolved in aqueous $NaHCO_3$. The aqueous layer was washed with ether to remove any residual organics. The aqueous layer was then acidified with concentrated HCl and the precipitate was collected and oven-dried (~80 °C) overnight to give 29.6 g (98.3 mmol, 97% yield) of the title compound. ^{1}H NMR (400 MHz, DMSO) δ (ppm) 13.60 (s, 2H), 7.68 (s, 2H), 1.28 (s, 9H).^{13}C NMR (100 MHz, DMSO) δ (ppm) 168.3, 150.7, 136.6, 127.8, 113.3, 34.6, 30.6. MS(ESI) m/z $[M-H]^-$ $C_{12}H_{12}O_4Br$ Calcd for: 298.99344 Found: 298.99225. M.P.:236.4-239.9 °C.

1.3 Synthesis of Dimethyl 2-Bromo-5-*tert*-butyl-isophthalate ($\mathbf{1^{Me}}$)

In a 100 mL three-necked round-bottom flask equipped with a magnetic stir bar and a reflux condenser was added 2-bromo-5-*tert*-butyl-isophthalic acid (8.0 g, 26.6 mmol), in 57.0 mL of methanol and 6 mL of H_2SO_4. The reaction mixture was heated to reflux for 24 h and neutralized with $NaHCO_3$ at 0 °C. The aqueous solution was washed several times with ether. The combined organic layers were dried over $MgSO_4$, filtered, and concentrated. Recrystallization from hexane gave 7.13 g (21.6 mmol, 82% yield) $\mathbf{1^{Me}}$ as white solid. ^{1}H NMR (400 MHz, $CDCl_3$) δ (ppm) 7.68 (s, 2H), 3.93 (s, 6H), 1.30 (s, 9H). ^{13}C NMR (100 MHz, $CDCl_3$) δ (ppm) 167.6, 150.9, 135.1, 129.6, 115.8, 77.48, 52.8, 34.8, 31.0. MS(ESI) m/z $[M+Na]^+$ $C_{18}H_{25}O_4BrNa$ Calcd for: 407.08284 Found: 407.08310. M.P.:100.3-101.1 °C.

1.4 Synthesis of diisopropyl 2-bromo-5-(*tert*-butyl) isophthalate (1^{iPr})

In a 100 mL two-necked round-bottom flask equipped with a magnetic stir bar and a reflux condenser was added 2-bromo-5-*tert*-butyl-isophthalic acid (8.0 g, 26.6 mmol), in 57.0 mL of isopropanol and 6.0 mL of H_2SO_4. The reaction mixture was heated to reflux for 24 h and neutralized with $NaHCO_3$. The aqueous solution was washed several times with diethyl ether. The combined organic layers were dried over $MgSO_4$ and filtered. Removal of solvent gave 7.96 g (24.4 mmol, 78% yield) **1^{iPr}** as colorless oil. ^{1}H NMR (400 MHz, $CDCl_3$) δ (ppm) 7.59 (s, 2H), 5.32 – 5.22 (m, 2H), 1.38 (d, *J* = 4 Hz, 12H), 1.30 (s, 9H). ^{13}C NMR (100 MHz, $CDCl_3$) δ (ppm) 166.9, 150.8, 135.9, 128.9, 115.0, 70.0, 34.8, 30.9 21.8. MS(ESI) m/z $[M+Na]^+$ $C_{14}H_{17}O_4BrNa$ Calcd for: 351.02024 Found: 351.02075.

General Procedure for Ullmann Coupling

The *para*-substituted diarylamine (1.0-1.2 eq. to the tridentate ligand precursor), dimethyl 2-bromo-5-*tert*-butyl-isophthalate (**1^{Me}**) or diisopropyl 2-bromo-5-(*tert*-butyl)isophthalate **(1^{iPr})**, potassium carbonate (1.5 eq. to the tridentate ligand precursor), and copper bronze (10-20 mol% eq. to the tridentate ligand precursor) were combined with *n*-Bu_2O in a round-bottom flask equipped with a magnetic stir bar and reflux condenser. The reaction was heated to 170-190 °C for 48-96 h under argon. The reaction was filtered, the solvent removed by vacuum distillation, and the residue purified by column chromatography.

1.5 Synthesis of dimethyl 2-(bis(4-chlorophenyl) amino)-5-(*tert*-butyl) isophthalate (2^{Me}a)

Bis(4-chlorophenyl) amine (7.30 g, 22.3 mmol) was coupled with dimethyl 2-Bromo-5-*tert*-butyl-isophthalate (**1^{Me}**) (6.92 g, 21.2 mmol) according to the above Ullmann procedure (120 mL of *n*-Bu_2O is selected for reaction solvent) for 67 h. The crude product was purified by flash chromatography using a 1:1 solution of CH_2Cl_2/hexane as the eluent to give 5.92 g (10.8 mmol, 51% yield) of the title compound as a pale-yellow solid. ^{1}H NMR (400 MHz, $CDCl_3$) δ (ppm) 7.81 (s, 2H), 7.14 (d, J = 4 Hz, 4H), 6.87 (d, J = 4 Hz, 4H), 3.54 (s, 6H), 1.36 (s, 9H). ^{13}C NMR (100 MHz, $CDCl_3$) δ (ppm) 167.6, 149.8, 145.5, 141.1, 132.1, 131.4, 129.1, 127.3, 123.3, 52.5, 35.0, 31.2. MS(ESI) m/z $[M+H]^+$ $C_{26}H_{26}O_4NCl_2$ Calcd for: 486.12334 Found: 486.12350. M.P.:158.0-159.5 °C.

1.6 Synthesis of dimethyl 2-(bis(4-(trifluoromethyl) phenyl) amino)-5-(*tert*-butyl) isophthalate (2^{Me}b)

Bis(4-(trifluoromethyl) phenyl) amine (610 mg, 2.00 mmol) was coupled with dimethyl 2-Bromo-5-*tert*-butyl-isophthalate (**1^{Me}**) (658 mg, 2.00 mmol) according to the above Ullmann procedure (15 mL of *n*-Bu_2O is selected for reaction solvent) for 96 h at 170 °C. The crude product was purified by flash chromatography using a 1:1 solution of CH_2Cl_2/hexane as the eluent to give 530 mg (0.958 mmol, 48% yield) of the title compound as a white solid: ^{1}H NMR (400 MHz, $CDCl_3$) δ (ppm) 7.91 (s, 2H), 7.45 (d, *J* = 8 Hz, 4H), 7.04 (d, *J* = 8 Hz, 4H), 3.53 (s, 6H), 1.38 (s, 9H). ^{13}C NMR (100 MHz, $CDCl_3$) δ (ppm) 167.1, 151.0, 149.2, 140.4, 132.3, 131.7, 126.3 (q, $^3J_{C\text{-}F}$ = 10 Hz), 124.4 (q, $^1J_{C\text{-}F}$ = 270 Hz), 124.3 (q, $^2J_{C\text{-}F}$ = 30 Hz), 121.7, 52.6, 35.1, 31.1. ^{19}F NMR (376 MHz, $CDCl_3$) δ -62.29. MS(ESI) m/z $[M+Na]^+$ $C_{28}H_{25}O_4NF_6Na$ Calcd for: 576.15800 Found: 576.15784.Elemental analysis: Calcld.: C, 60.76; H, 4.55; N, 2.53; Found: C, 61.14; H, 4.54; N, 2.61. M.P.:183.8-185.2 °C.

1.7 Synthesis of diisopropyl 2-(bis(4-chlorophenyl) amino)-5-(*tert*-butyl) isophthalate (2^{iPr}a)

Bis(4-chlorophenyl) amine (289 mg, 1.21 mmol) was coupled with diisopropyl 2-bromo-5-(*tert*-butyl) isophthalate **(1^{iPr})** (445 mg, 1.15 mmol) according to the above Ullmann procedure for 120 h. The crude product was purified by flash chromatography using a 1:1 solution of CH_2Cl_2/hexane as the eluent to give 339 mg (0.625 mmol, 54% yield) of the title compound as a pale-yellow solid. ^{1}H NMR (400MHz, $CDCl_3$) δ (ppm) 7.73 (s, 2H), 7.12 (d, *J* = 8 Hz, 4H), 6.90 (d, *J* = 8 Hz, 4H), 4.85 (m, 2H), 1.36 (s, 9H), 1.04 (d, *J* =8 Hz, 12H). ^{13}C NMR (100 MHz, $CDCl_3$) δ (ppm) 166.5, 149.9, 145.3, 140.6, 133.4, 130.4, 128.9, 126.9, 123.1, 69.5, 34.9, 31.2, 21.6. MS(ESI) m/z $[M+H]^+$ $C_{30}H_{34}O_4NCl_2$ Calcd for: 542.18594 Found: 542.18604. Elemental analysis: Calcld.: C, 66.42; H, 6.13; N, 2.58; Found: C, 66.80; H, 6.29; N, 2.63. M.P.:144.8-145.2 °C.

1.8 Synthesis of diisopropyl 2-(bis(4-(trifluoromethyl) phenyl) amino)-5-(*tert*-butyl) isophthalate (2^{iPr}b)

Bis(4-(trifluoromethyl) phenyl) amine (370 mg, 1.21 mmol) was coupled with diisopropyl 2-bromo-5-(*tert*-butyl) isophthalate **(1^{iPr})** (562 mg, 1.45 mmol) according to the above Ullmann procedure for 98 h. The crude product was purified by flash chromatography using a 1:1 solution of CH_2Cl_2/hexane as the eluent to give 405 mg (0.664 mmol, 55% yield) of the title compound as a pale-yellow solid. ^{1}H NMR (400 MHz, $CDCl_3$) δ (ppm) 7.80 (s, 2H), 7.44 (d, *J* = 8 Hz, 4H), 7.07 (d, *J* = 8 Hz, 4H), 4.85 (m, *J* = 24 Hz, 2H), 1.38 (s, 9H), 0.99 (d, *J* = 4 Hz, 12H). ^{13}C NMR (100 MHz, $CDCl_3$) δ (ppm) 166.1, 150.9, 149.1, 140.1, 133.4, 130.7, 126.2 (q, $^3J_{C\text{-}F}$ = 10 Hz), 124.5 (q, $^1J_{C\text{-}F}$ = 270 Hz), 124.0 (q, $^2J_{C\text{-}F}$ = 30 Hz), 121.6, 69.7, 35.0, 31.2, 21.4. ^{19}F NMR (376 MHz, $CDCl_3$) δ (ppm) -62.45. MS(ESI) m/z $[M+Na]^+$ $C_{32}H_{33}O_4NF_6Na$ Calcd for: 632.22060 Found: 632.22052 Elemental analysis: Calcld.: C, 63.05; H, 5.46; N, 2.30; Found: C, 62.99; H, 5.25; N, 2.28. M.P.:188.8-190.1 °C.

1.9 Reaction of 2^{Me}a with (2,4-$Br_2C_6H_4)_3N^{\bullet+}SbCl_6^-$ (3^{Me}a)

A solution of **2^{Me}a** (49 mg, 0.10 mmol) and (2,4-$Br_2C_6H_4)_3N^{\bullet+}SbCl_6^-$ (105 mg, 0.100 mmol) in dry CH_2Cl_2 (5 mL) was stirred for 30 mins at room temperature. The solution color was changed to dark blue. After the removal of solvent, the residue was washed with Et_2O to give compound **3^{Me}a** as a dark green solid (60 mg, 0.072 mmol, 72%). Purple crystals of **3^{Me}a** suitable for X-ray analysis were obtained by recrystallization from CH_2Cl_2 /hexane under light-shielded condition.

1.10 Reaction of 2^{Me}b with $(2,4\text{-}Br_2C_6H_4)_3N^{\bullet+}SbCl_6^-$ (3^{Me}b)

A solution of **2^{Me}b** (53 mg, 0.10 mmol) and $(2,4\text{-}Br_2C_6H_4)_3N^{\bullet+}SbCl_6^-$ (105 mg, 0.10 mmol) in dry CH_2Cl_2 (5.0 mL) was stirred for 30 mins at room temperature. The solution color was changed to dark blue. After the removal of solvent, the residue was washed with Et_2O to give compound **3^{Me}b** as a dark green solid (65 mg, 0.073 mmol, 73%).

1.11 Reaction of 2^{iPr}a with $(2,4\text{-}Br_2C_6H_4)_3N^{\bullet+}SbCl_6^-$($3^{iPr}$a)

A solution of **2^{iPr}a** (20 mg, 0.037 mmol) and $(2,4\text{-}Br_2C_6H_4)_3N^{\bullet+}SbCl_6^-$ (39 mg, 0.037 mmol) in dry CH_2Cl_2 (5 mL) was stirred for 30 mins at room temperature. The solution color was changed to dark blue. After the removal of solvent, the residue was washed with Et_2O to give compound **3^{iPr}a** as a dark green solid (20 mg, 0.023 mmol, 62%). Purple crystals of **3^{iPr}a** suitable for X-ray analysis were obtained by recrystallization from CH_2Cl_2 / hexane under light-shielded condition.

1.12 Reaction of 2^{iPr}b with $(2,4\text{-}Br_2C_6H_4)_3N^{\bullet+}SbCl_6^-$($3^{iPr}$b)

A solution of **2^{iPr}b** (35 mg, 0.057 mmol) and $(2,4\text{-}Br_2C_6H_4)_3N^{\bullet+}SbCl_6^-$ (60 mg, 0.057 mmol) in dry CH_2Cl_2 (5 mL) was stirred for 30 mins at room temperature. The solution color was changed to dark blue. After the removal of solvent, the residue was washed with Et_2O to give compound **3^{iPr}b** as a dark green solid (58 mg, 0.062 mmol, 92%).

2. UV-Vis, EPR and CV spectra

2.1 UV-Vis and Emission spectra

UV/Vis spectrum of 0.01 mM solution of **2^{Me}a-b**, **2^{iPr}a-b** and **3^{Me}a-b** and **3^{iPr}a-b** in DCM was recorded on UV-1650PC (SHIMADZU) and HORIBA FluoroMax-4 spectrophotometer in ambient atmosphere at room temperature. The obtained spectrum was illustrated in in Figure S1 and Figure S2.

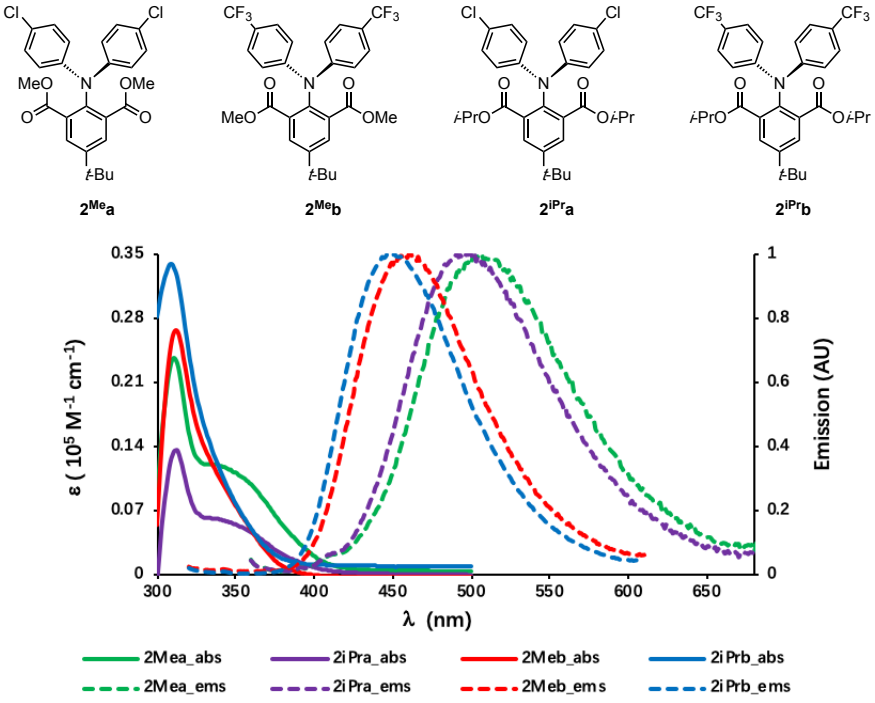

Figure S1. Absorption spectra (solid) and emission spectra (dashed) of 10^{-5} M **2^{Me}a-b** and **2^{iPr}a-b** in CH_2Cl_2 at 25 °C.

Table S1 Summary of absorption and emission spectra

Compound	2^{Me}a	2^{Me}b	2^{iPr}a	2^{iPr}b
Wavelength (nm)	311	312	312	309
Max. ε (10^5 M^{-1} cm^{-1})	0.237	0.266	0.136	0.339
Quantum Yield	3.22	3.50	9.43	13.95
Lifetime(318nm) (ns)	14.98714	13.47508	7.182881	4.996558

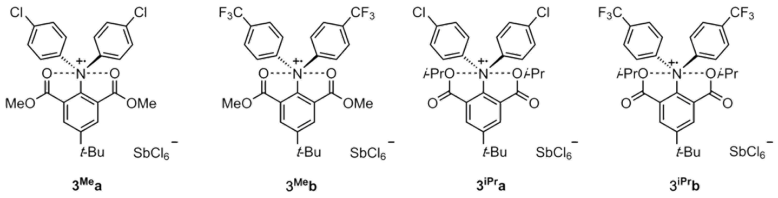

$3^{Me}a$ $3^{Me}b$ $3^{iPr}a$ $3^{iPr}b$

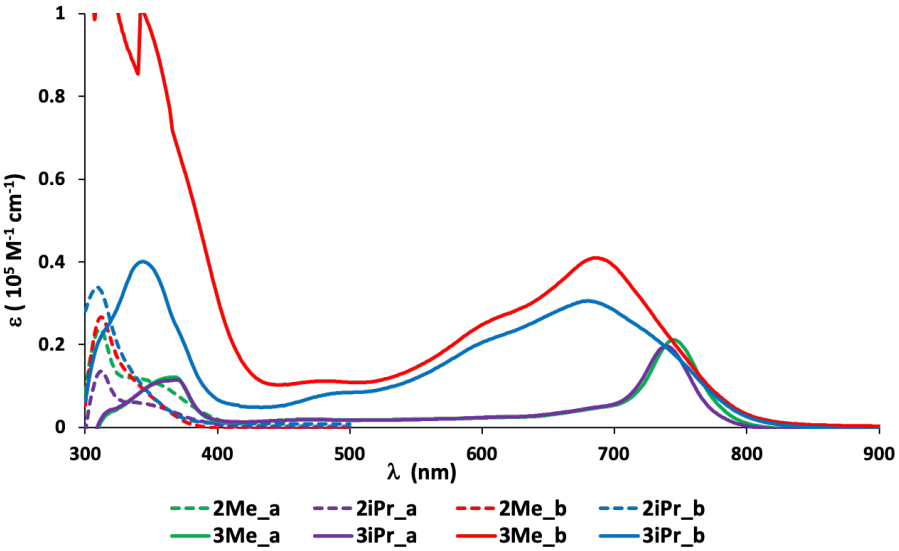

Figure S2. Absorption spectra of 10^{-5} M 2^{Me}**a-b** and 2^{iPr}**a-b** (solid), 3^{Me}**a-b** and 3^{iPr}**a-b** (dashed) in CH_2Cl_2 at 25 °C.

Table S2 Summary of absorption spectra

Compound	3^{Me}**a**	3^{Me}**b**	3^{iPr}**a**	3^{iPr}**b**
Wavelength (nm)	745	688	739	681
max. ε (10^5 M^{-1} cm^{-1})	0.212	0.696	0.197	0.305

2.2 Electron paramagnetic resonance (EPR)

The electron paramagnetic resonance (EPR) spectra of **3^{Me}a-b** and **3^{iPr}a-b** were measured by using a Bruker ELEXSYS E500 spectrometer at room temperature. All samples were prepared as a 10^{-5}~10^{-4} mM solution in CH_2Cl_2. After freeze-pump-thaw cycles, the solution sample in a quartz tube was sealed by frame. Spectral simulation was performed using EasySpin, which is a MATLAB toolbox meant for this.

Table S3 Spin Hamiltonian parameters estimated from the spectral simulation for **3^{Me}a-b** and **3^{iPr}a-b**. The number of equivalent protons is noted in brackets.

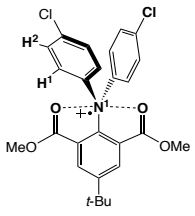

3^{Me}a

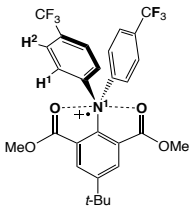

3^{Me}b

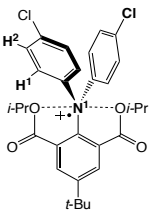

3^{iPr}a

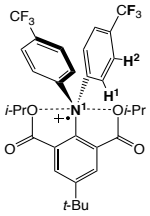

3^{iPr}b

	3^{Me}a	**3^{Me}b**	**3^{iPr}a**	**3^{iPr}b**	**Equivalency**
g	2.0042	2.0028	2.0042	2.0035	–
A_{N1} / MHz	26.8	29.9	27.2	29.9	1
A_{H1} / MHz	7.2	14.7	7.7	14.4	4
A_{H2} / MHz	4.6	7.5	4.5	7.4	4
A_{Cl} / MHz	<1	–	<1	–	2
A_F / MHz	–	4.1	–	3.9	6

2.3 Cyclic voltammetry

Cyclic voltammetry measurement of **2^{Me}a-b** and **2^{iPr}a-b** (1.0 mM) was performed by using an ALS 600D potentiostat / galvanostat in DCM solution containing 100 mM of [nBu_4N] [PF_6] with a scan rate of 100 mV/s in ambient atmosphere at room temperature. A three-electrode cell, which was equipped with a Pt disk working electrode, a Pt wire counter electrode, and SCE reference electrode, was used. The half wave potentials of **2^{Me}a-b** and **2^{iPr}a-b** was compensated with that of ferrocene/ferrocenium redox cycle, which is +0.46 V (vs. SCE). The cyclic voltammogram is illustrated in Figure S3.

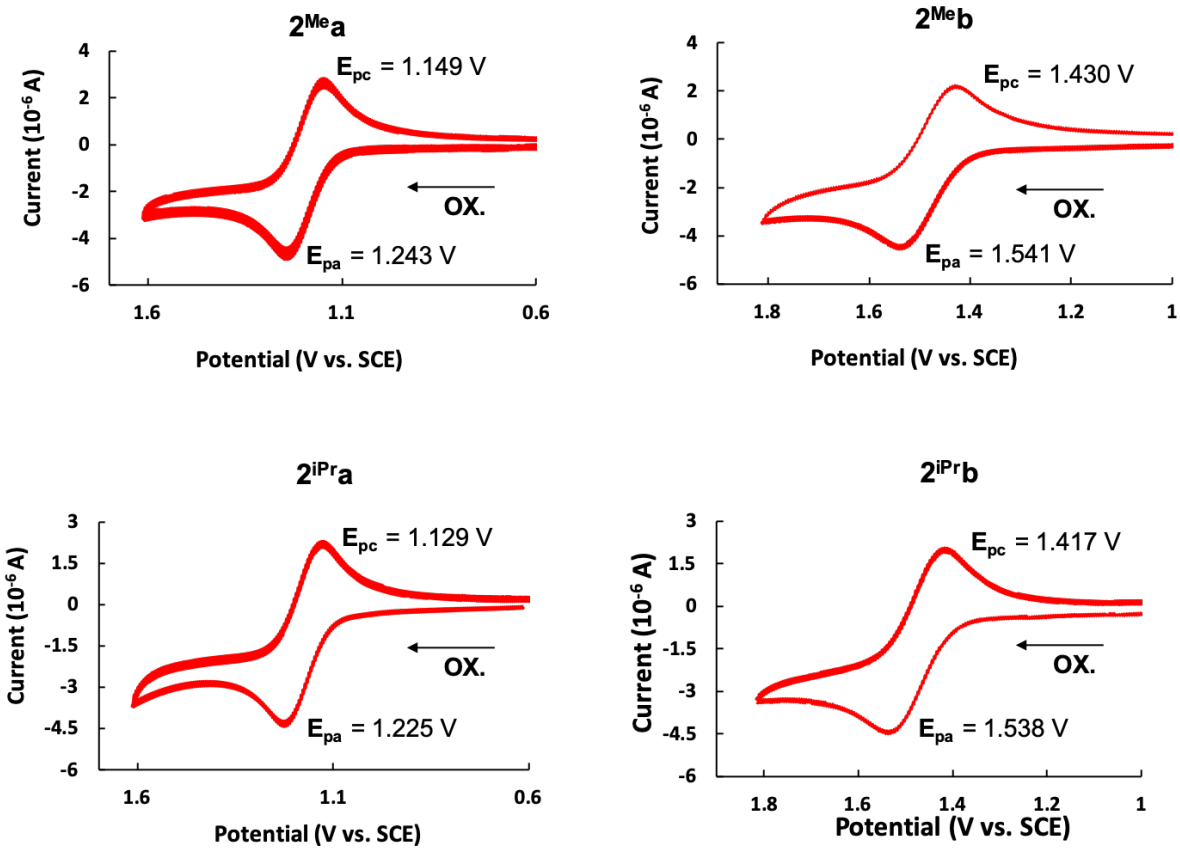

Figure S3. Cyclic voltammogram of a 1.0 mM solution of **2^{Me}a-b** and **2^{iPr}a-b** in DCM using 100 mM of [nBu_4N] [PF_6] as the supporting electrolyte.

Table S4. Formal potentials of neutral compounds.

Compound	E_{pa} / v	E_{pc} / v	Formal potentials / v
2^{Me}a	1.243	1.149	1.196
2^{Me}b	1.541	1.430	1.485
2^{iPr}a	1.225	1.129	1.177
2^{iPr}b	1.538	1.417	1.477

3. Crystal Structure Determination

Crystals suitable for X-ray structural determination were mounted on a Bruker SMART APEXII CCD diffractometer. Samples were irradiated with graphite monochromated Mo-Kα radiation (λ= 0.71073 Å) at 173 K for data collection. The data were processed using the APEX program suite. All structures were solved by the *SHELXT* program (*ver.* 2014/5). Refinement on F^2 was carried out by full-matrix least-squares using the *SHELXL* in the *SHELX* software package (ver. 2014/7) [1] and expanded using Fourier techniques. All non-hydrogen atoms were refined using anisotropic thermal parameters. The hydrogen atoms were assigned to idealized geometric positions and included in the refinement with isotropic thermal parameters. The SHELXL was interfaced with ShelXle GUI (ver. 742) for most of the refinement steps. [2] The pictures of molecules were prepared using Pov-Ray 3.7.0.[3] The crystallographic data are summarized in Table S5. CCDC-1945530-1945536 contain the supplementary crystallographic data for this paper.

Table S5. Selected X-ray parameter of **1^{Me}** ,**2^{Me}a-b**, **2^{iPr}a-b**, **3^{Me}a** and **3^{iPr}a**.

CCDC	**1^{Me}** 1945530	**2^{Me}a** 1945531	**2^{Me}b** 1945532	**3^{Me}a** 1945533	**2^{iPr}a** 1945534	**2^{iPr}b** 1945535	**3^{iPr}a** 1945536
Formula	$C_{14}H_{17}BrO$	$C_{26}H_{25}Cl_2NO_4$	$C_{28}H_{25}F_6NO_4$	$C_{26}H_{25}Cl_8NO_4Sb$	$C_{30}H_{33}Cl_2NO_4$	$C_{32}H_{33}F_6NO_4$	$C_{30}H_{33}Cl_8NO_4Sb$
Mol wt	329.18	486.37	553.49	820.82	542.47	609.59	876.92
Crystal system	Orthorhombic	Orthorhombic	Monoclinic	Monoclinic	Triclinic	Triclinic	Monoclinic
Space group	Pbcn	Pbca	$P2_1/n$	$P2_1/n$	P-1	P-1	$P2_1/n$
***a*, Å**	21.874(5)	18.3830(16)	11.7241(3)	11.6398(8)	11.840(2)	10.0890(4)	12.156(3)
***b*, Å**	15.366(3)	13.3271(12)	12.3047(3)	18.4868(13)	14.543(3)	11.8293(5)	15.548(3)
***c*, Å**	8.915(3)	20.1022(18)	18.3432(5)	16.2027(11)	18.231(3)	13.7884(6)	19.482(4)
***α*, deg**	90	90	90	90	97.047(3)	97.5670(10)	90
***β*, deg**	90	90	100.0770(10)	109.070(3)	105.059(3)	107.7540(10)	90.770(4)
***γ*, deg**	90	90	90	90	102.364(3)	95.2740(10)	90
V, Å^3	2996.4(12)	4924.9(8)	2605.40(12)	3295.2(4)	2907.6(9)	1538.29(11)	3681.6(13)
Z	8	8	4	4	4	2	4
D_{calc}, Mg/m^3	1.459	1.312	1.411	1.655	1.239	1.316	1.582
Abs coeff, mm^{-1}	2.750	0.296	0.122	1.518	0.257	0.110	1.365
***F*(000)**	1344	2032	1144	1628	1144	636	1756
Temp, K	173(2)	173(2)	173(2)	173(2)	173(2)	173(2)	173(2)
Reflections	33840	44338	12410	15559	14070	18837	20884
Independent	3737	4249	4485	5614	10099	7482	8431
***R*int**	0.0358	0.0348	0.0222	0.0246	0.0334	0.0452	0.0860
Parameters	177	303	413	366	689	451	411
***R1* [$I > 2\sigma(I)$]**	0.0272	0.0384	0.0385	0.0312	0.0610	0.0406	0.0573
wR_2 (all data)	0.0727	0.1076	0.1032	0.0800	0.2302	0.1114	0.1058

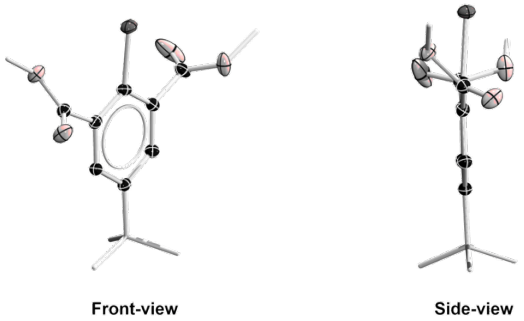

Figure S4. Molecular structures of $\mathbf{1^{Me}}$ obtained from single-crystal X-ray diffraction analysis. Thermal ellipsoids are displayed at 30% probability. Hydrogen atoms are omitted for clarity.

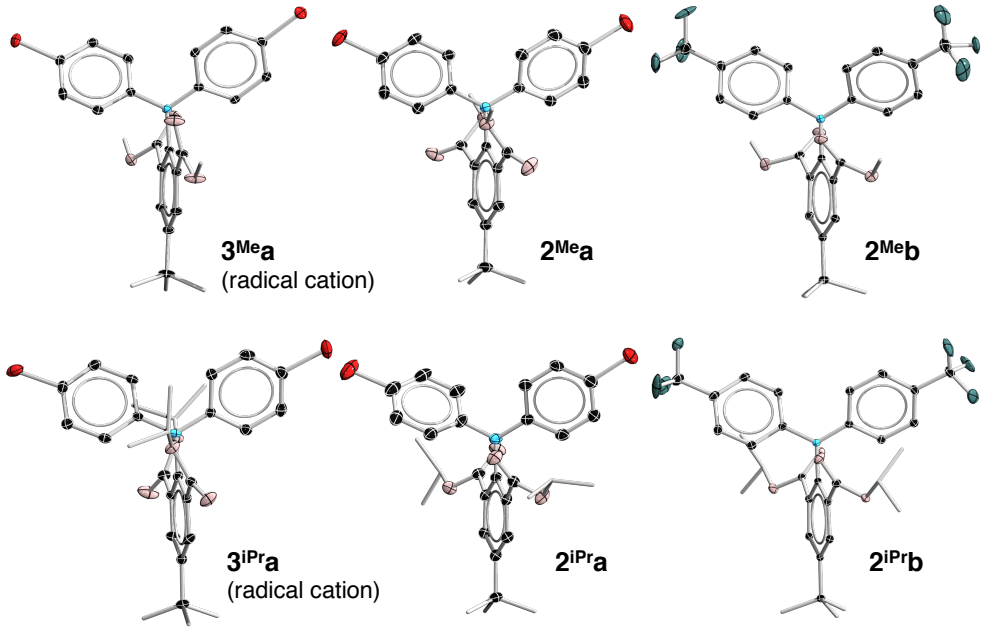

Figure S5. Molecular structure of $\mathbf{2^{Me}a\text{-}b}$, $\mathbf{2^{iPr}a\text{-}b}$, $\mathbf{3^{Me}a}$ and $\mathbf{3^{iPr}a}$ (Side-view) obtained from single-crystal X-ray diffraction analysis. Thermal ellipsoids are displayed at 30% probability. Hydrogen atoms are omitted for clarity.

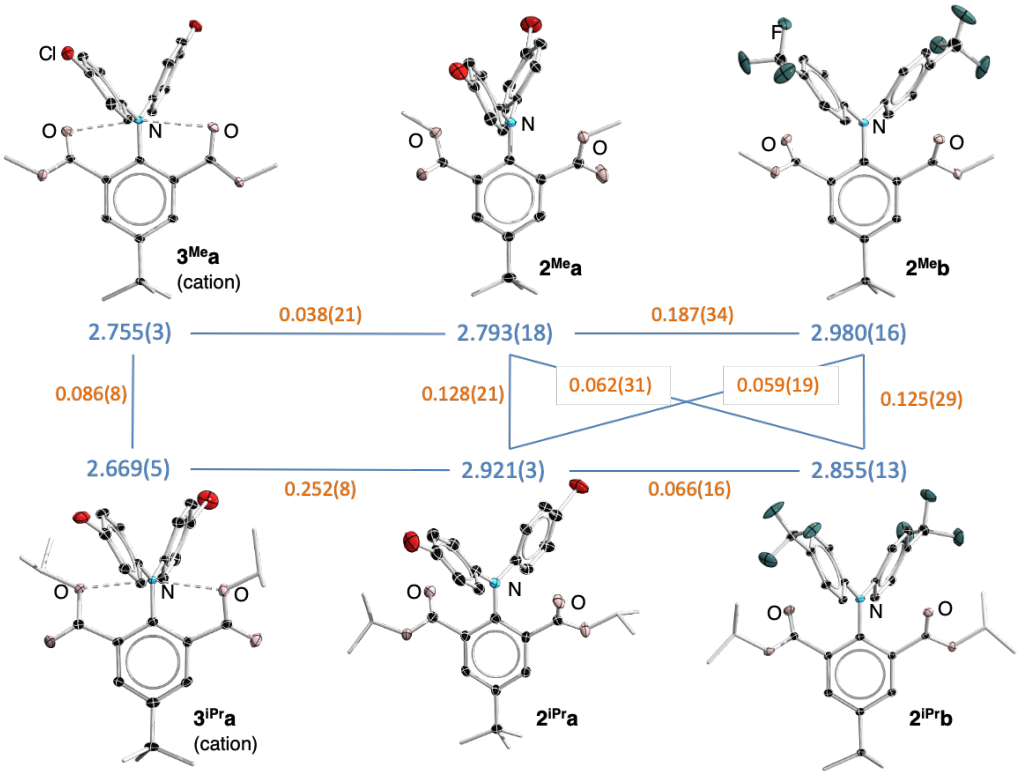

Figure S6. The difference of N-O bond length between **2^{Me}a-b**, **2^{iPr}a-b**, **3^{Me}a** and **3^{iPr}a**: average N-O distances (blue); differences of NO distance (orange).

4. DFT calculation

4.1 Optimized geometries

Geometry optimizations were performed at the RCAM- and UCAM-B3LYP-D3/def2-SVP, B3PW91/6-31G(d) and UB3PW91/6-31G(d), B3LYP/6-31G(d,p) and UB3LYP/6-31G(d,p), B3LYP/cc-pVDZ and UB3LYP/cc-pVDZ levels for **2** and **3**, respectively, using Gaussian 09 program package. Here, IEF-PCM method was employed in order to consider solvent (CH_2Cl_2) effects.

Single point calculations at the RCAM- and UCAM-B3LYP-D3/def2-SVP levels were performed using ORCA 4.2 program package [4], where C-PCM method was employed for solvent effects. Natural population analysis (NPA) and atoms in molecules (AIM) analysis were performed using the NBO 6.0[5] and Multiwfn 3.6[6] program packages, respectively. For the domain-based local pair-natural orbital coupled-cluster singles and doubles (DLPNO-CCSD)/def2-SVP calculations [7], the options "NormalPNO" and "VeryTightSCF" as well as def2-SVP/C and def2/JK auxiliary basis were employed.

Table S6. Selected calculated bond lengths (Å), angles and dihedral angles [°], and net NPA charges q [–] for **2^{Me}a-b**, **2^{iPr}a-b, 3^{Me}a** and **3^{iPr}a** at the RCAM- and UCAM-B3LYP-D3/def2-SVP levels in **2** and **3**, respectively.

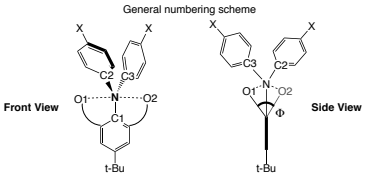

Parameters	Ionic radical	Neutral		Ionic radical	Neutral	
	3^{Me}a	**2^{Me}a**	**2^{Me}b**	**3^{iPr}a**	**2^{iPr}a**	**2^{iPr}b**
Coord.	(C***O***)	(***O***Me)	(C***O***)	(***O***iPr)	(C***O***)	(C***O***)
N-O1	2.684	2.734	2.795	2.673	2.885	2.882
N-O2	2.686	2.734	2.802	2.676	2.889	2.886
N-O_{Ave}	2.684	2.734	2.798	2.674	2.887	2.884
N-C1	1.435	1.417	1.420	1.439	1.416	1.419
N-C2	1.387	1.405	1.403	1.387	1.408	1.405
N-C3	1.388	1.405	1.401	1.388	1.407	1.404
$\Sigma N\alpha$	360.0	360.0	360.0	360.0	360.0	360.0
Φ_{OCCO}	39.1	67.2	56.3	47.0	73.6	74.4
q(N)	–0.270	–0.502	–0.497	–0.275	–0.498	–0.493
q(O1)	–0.645	–0.648	–0.637	–0.602	–0.643	–0.643
q(O2)	–0.645	–0.648	–0.638	–0.602	–0.643	–0.643
q(C1)	0.178	0.212	0.217	0.165	0.214	0.208
q(C2)	0.170	0.175	0.198	0.176	0.173	0.194
q(C3)	0.171	0.175	0.200	0.174	0.173	0.195

Table S7. Selected calculated bond lengths (Å), angles and dihedral angles [°] for **2^{Me}a-b**, **2^{iPr}a-b**, **3^{Me}a** and **3^{iPr}a** at the B3PW91/6-31G(d) in **2** and UB3PW91/6-31G(d) in **3**, respectively.

Parameters	Ionic radical	Neutral		Ionic radical	Neutral	
	3^{Me}a	**2^{Me}a**	**2^{Me}b**	**3^{iPr}a**	**2^{iPr}a**	**2^{iPr}b**
Coord.	(C***O***)	(***O***Me)	(C***O***)	(***O***iPr)	(C***O***)	(C***O***)
N-O1	2.727	2.795	2.871	2.798	2.884	2.855
N-O2	2.727	2.796	2.873	2.860	2.870	2.858
N-O_{Ave}	2.727	2.796	2.872	2.820	2.877	2.857
N-C1	1.436	1.42	1.418	1.432	1.416	1.419
N-C2	1.393	1.409	1.408	1.394	1.410	1.406
N-C3	1.393	1.409	1.407	1.394	1.409	1.407
ΣNα	360.0	360.0	360.0	360.0	360.0	360.8
Φ_{OCCO}	45.3	69.1	66.5	74.2	69.2	65.4

Table S8. Selected calculated bond lengths (Å), angles and dihedral angles [°] for **2^{Me}a-b**, **2^{iPr}a-b**, **3^{Me}a** and **3^{iPr}a** at the B3LYP/6-31G(d,p) in **2** and UB3LYP/6-31G(d,p) in **3**, respectively.

Parameters	Ionic radical	Neutral		Ionic radical	Neutral	
	3^{Me}a	**2^{Me}a**	**2^{Me}b**	**3^{iPr}a**	**2^{iPr}a**	**2^{iPr}b**
Coord.	(C***O***)	(***O***Me)	(C***O***)	(***O***iPr)	(C***O***)	(C***O***)
N-O1	2.733	2.801	2.876	2.788	2.885	2.869
N-O2	2.734	2.802	2.877	2.845	2.892	2.876
N-O_{Ave}	2.733	2.801	2.876	2.816	2.888	2.872
N-C1	1.443	1.426	1.424	1.440	1.422	1.425
N-C2	1.398	1.415	1.413	1.399	1.415	1.413
N-C3	1.398	1.415	1.413	1.399	1.416	1.412
ΣNα	360.0	360.0	360.0	360.0	360.0	360.0
Φ_{OCCO}	43.7	68.6	65.3	70.0	69.5	67.2

Table S9. Selected calculated bond lengths (Å), angles and dihedral angles [°] for **2^{Me}a-b**, **2^{iPr}a-b**, **3^{Me}a** and **3^{iPr}a** at the B3LYP/cc-pVDZ in **2** and UB3LYP/cc-pVDZ in **3**, respectively.

Parameters	Ionic radical	Neutral		Ionic radical	Neutral	
	3^{Me}a	**2^{Me}a**	**2^{Me}b**	**3^{iPr}a**	**2^{iPr}a**	**2^{iPr}b**
Coord.	(C***O***)	(***O***Me)	(C***O***)	(***O***iPr)	(C***O***)	(C***O***)
N-O1	2.722	2.771	2.847	2.773	2.857	2.835
N-O2	2.723	2.772	2.848	2.824	2.866	2.844
N-O_{Ave}	2.722	2.771	2.847	2.798	2.861	2.839
N-C1	1.444	1.428	1.426	1.442	1.423	1.427
N-C2	1.398	1.415	1.414	1.399	1.416	1.413
N-C3	1.399	1.415	1.413	1.399	1.415	1.412
ΣNα	360.0	360.0	360.0	360.0	360.0	360.0
Φ_{OCCO}	38.3	59.5	57.6	62.8	62.7	58.8

4.2 TD-DFT calculation

TDDFT calculation was carried out at the B3LYP/cc-pVDZ level in **2** and at UB3LYP/cc-pVDZ level in **3** using the *Gaussian 09* program. CH_2Cl_2 for solvent effect.

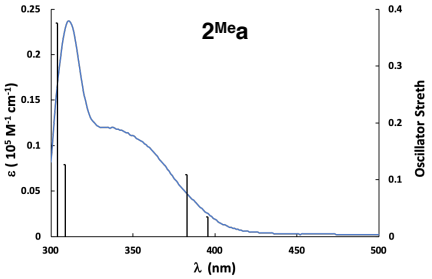

2^{Me}a HOMO 127 LUMO 128

Excited State 1:	Singlet-A	3.1339 eV	395.62 nm	f=0.0346	<S**2>=0.000
127 ->128	0.70095				
Excited State 2:	Singlet-A	3.2374 eV	382.97 nm	f=0.1086	<S**2>=0.000
127 ->129	0.70014				
Excited State 3:	Singlet-A	4.0178 eV	308.59 nm	f=0.1265	<S**2>=0.000
127 ->130	0.48970				
127 ->131	0.49809				
Excited State 4:	Singlet-A	4.0805 eV	303.85 nm	f=0.3753	<S**2>=0.000
127 ->130	0.50091				
127 ->131	-0.48364				
Excited State 5:	Singlet-A	4.3549 eV	284.70 nm	f=0.0280	<S**2>=0.000
127 ->132	0.68570				
Excited State 6:	Singlet-A	4.7402 eV	261.56 nm	f=0.0118	<S**2>=0.000
121 ->128	-0.14620				
122 ->128	-0.12228				
122 ->129	0.16698				
123 ->128	-0.24082				
124 ->129	0.33066				
125 ->128	0.36901				
126 ->128	-0.17813				
126 ->129	0.28509				

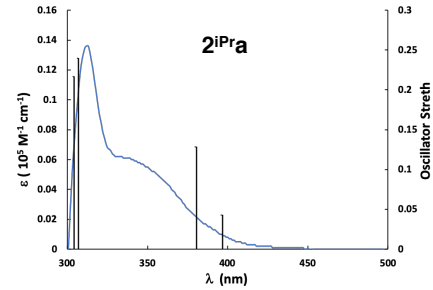

2^{iPr}a HOMO 143 LUMO 144

Excited State 1:	Singlet-A	3.1253 eV	396.71 nm	f=0.0431	<S**2>=0.000
143 ->144	0.70139				
Excited State 2:	Singlet-A	3.2589 eV	380.45 nm	f=0.1286	<S**2>=0.000
143 ->145	0.70047				
Excited State 3:	Singlet-A	4.0411 eV	306.81 nm	f=0.2400	<S**2>=0.000
143 ->146	0.60353				
143 ->147	-0.34482				
Excited State 4:	Singlet-A	4.0763 eV	304.16 nm	f=0.2169	<S**2>=0.000
143 ->146	0.35085				
143 ->147	0.60431				
Excited State 5:	Singlet-A	4.3770 eV	283.27 nm	f=0.0317	<S**2>=0.000
143 ->148	0.68453				
Excited State 6:	Singlet-A	4.7239 eV	262.46 nm	f=0.0244	<S**2>=0.000
136 ->145	0.15938				
137 ->144	-0.19568				
138 ->144	-0.12125				
138 ->145	0.11356				
139 ->144	-0.26758				
140 ->145	-0.19364				
141 ->144	0.50291				
142 ->144	-0.10948				
142 ->145	0.11591				

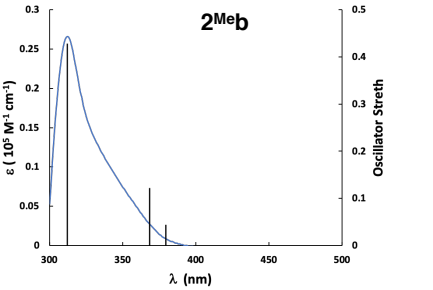

2^{Me}b HOMO 143 LUMO 144

Excited State 1:	Singlet-A	3.2665 eV	379.56 nm	f=0.0442	<S**2>=0.000
143 ->144	0.69867				
Excited State 2:	Singlet-A	3.3646 eV	368.50 nm	f=0.1217	<S**2>=0.000
143 ->145	0.69844				
Excited State 3:	Singlet-A	3.9744 eV	311.96 nm	f=0.4288	<S**2>=0.000
143 ->146	0.69913				
Excited State 4:	Singlet-A	4.2481 eV	291.86 nm	f=0.0114	<S**2>=0.000
142 ->146	-0.10824				
143 ->147	0.68630				
Excited State 5:	Singlet-A	4.5535 eV	272.28 nm	f=0.0290	<S**2>=0.000
141 ->146	-0.12622				
142 ->145	-0.10370				
143 ->148	0.65771				
143 ->149	0.11286				
Excited State 6:	Singlet-A	4.7144 eV	262.99 nm	f=0.0156	<S**2>=0.000
136 ->145	0.16362				
137 ->144	0.14972				
139 ->144	-0.16657				
139 ->145	0.11536				
140 ->144	-0.29742				
141 ->145	0.19374				
142 ->144	0.50254				

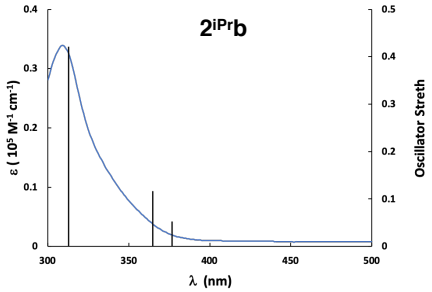

2^{iPr}b HOMO 159 LUMO 160

Excited State 1:	Singlet-A	3.2910 eV	376.74 nm	f=0.0523	<S**2>=0.000
159 ->160	0.69757				
Excited State 2:	Singlet-A	3.3987 eV	364.80 nm	f=0.1171	<S**2>=0.000
159 ->161	0.69749				
Excited State 3:	Singlet-A	3.9637 eV	312.80 nm	f=0.4213	<S**2>=0.000
159 ->162	0.69874				
Excited State 4:	Singlet-A	4.2374 eV	292.60 nm	f=0.0102	<S**2>=0.000
158 ->162	0.10096				
159 ->163	0.68683				
Excited State 5:	Singlet-A	4.5454 eV	272.77 nm	f=0.0265	<S**2>=0.000
157 ->162	-0.11625				
159 ->164	0.66042				
159 ->165	-0.10638				
Excited State 6:	Singlet-A	4.7088 eV	263.30 nm	f=0.0154	<S**2>=0.000
152 ->161	-0.17221				
153 ->160	-0.16031				
155 ->160	-0.13010				
156 ->160	-0.31352				
157 ->161	0.19257				
158 ->160	0.50540				

Figure S7. TD-DFT of optimized **2^{Me}a-b** and **2^{iPr}a-b** at the B3LYP/cc-pVDZ level. Experimental absorption (blue) and Oscillator strength (black).

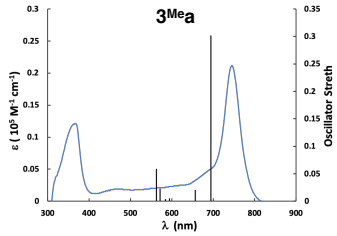

^{3Me}a HOMO 126 SOMO 127 LUMO 128
Excited State 1: 2.022-A 1.7870 eV 693.81 nm f=0.3020 <S**2>=0.772
127A ->130A 0.11635
126B ->127B 0.98763
Excited State 2: 2.029-A 1.8886 eV 656.47 nm f=0.0204 <S**2>=0.779
122B ->127B -0.30756
125B ->127B 0.94095
Excited State 3: 2.026-A 2.0854 eV 594.52 nm f=0.0051 <S**2>=0.776
122B ->127B 0.60043
123B ->127B -0.32339
124B ->127B 0.69966
125B ->127B 0.18288
Excited State 4: 2.032-A 2.1222 eV 584.22 nm f=0.0038 <S**2>=0.783
120B ->127B -0.15661
121B ->127B 0.87331
123B ->127B -0.39063
124B ->127B -0.21555
Excited State 5: 2.027-A 2.1694 eV 571.52 nm f=0.0229 <S**2>=0.778
121B ->127B 0.43403
122B ->127B -0.19426
123B ->127B 0.69022
124B ->127B 0.51256
125B ->127B -0.15934
Excited State 6: 2.030-A 2.2034 eV 562.70 nm f=0.0588 <S**2>=0.780
121B ->127B 0.11656
122B ->127B 0.70196
123B ->127B 0.50029
124B ->127B -0.43076
125B ->127B 0.20796

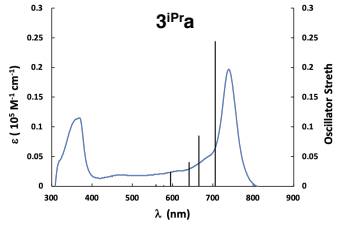

^{iPr}a HOMO 142 SOMO 143 LUMO 144
Excited State 1: 2.021-A 1.7562 eV 705.96 nm f=0.2439 <S**2>=0.771
140B ->143B -0.12106
141B ->143B -0.17832
142B ->143B 0.96484
Excited State 2: 2.027-A 1.8644 eV 665.01 nm f=0.0854 <S**2>=0.777
138B ->143B -0.28012
140B ->143B -0.21669
141B ->143B 0.91464
142B ->143B 0.14691
Excited State 3: 2.027-A 1.9355 eV 640.58 nm f=0.0406 <S**2>=0.777
137B ->143B -0.12906
138B ->143B 0.16597
140B ->143B 0.92676
141B ->143B 0.24452
142B ->143B 0.15799
Excited State 4: 2.032-A 2.0830 eV 595.21 nm f=0.0242 <S**2>=0.782
138B ->143B 0.90863
139B ->143B -0.21603
140B ->143B -0.23293
141B ->143B 0.23759
Excited State 5: 2.032-A 2.1455 eV 577.89 nm f=0.0015 <S**2>=0.782
136B ->143B 0.19617
137B ->143B 0.94659
139B ->143B 0.17992
140B ->143B 0.12431
Excited State 6: 2.023-A 2.2194 eV 558.63 nm f=0.0025 <S**2>=0.774
137B ->143B -0.17120
138B ->143B 0.23024
139B ->143B 0.95468

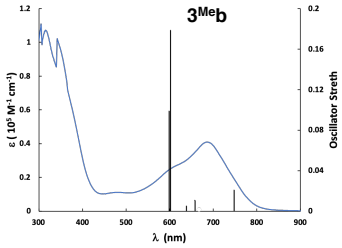

^{Me}b HOMO 142 SOMO 143 LUMO 144
Excited State 1: 2.030-A 1.6575 eV 748.02 nm f=0.0210 <S**2>=0.780
137B ->143B 0.21085
140B ->143B -0.13037
142B ->143B 0.95931
Excited State 2: 2.031-A 1.8563 eV 667.90 nm f=0.0014 <S**2>=0.781
137B ->143B -0.20948
138B ->143B -0.17392
140B ->143B 0.87189
141B ->143B -0.33614
142B ->143B 0.19920
Excited State 3: 2.035-A 1.8836 eV 658.23 nm f=0.0106 <S**2>=0.785
136B ->143B 0.13152
137B ->143B -0.20716
138B ->143B 0.68537
139B ->143B -0.15388
140B ->143B 0.30655
141B ->143B 0.58487
Excited State 4: 2.030-A 1.9420 eV 638.44 nm f=0.0051 <S**2>=0.781
138B ->143B -0.55564
139B ->143B 0.41012
140B ->143B 0.18921
141B ->143B 0.68961
Excited State 5: 2.037-A 2.0585 eV 602.31 nm f=0.1786 <S**2>=0.788
143A ->146A -0.10606
137B ->143B 0.24088
138B ->143B 0.40408
139B ->143B 0.82941
140B ->143B 0.10650
141B ->143B -0.21397
Excited State 6: 2.034-A 2.0695 eV 599.09 nm f=0.0988 <S**2>=0.785
137B ->143B 0.88974
139B ->143B -0.30287
140B ->143B 0.26822
142B ->143B -0.14939

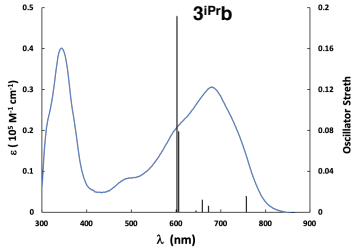

^{iPr}b HOMO 158 SOMO 159 LUMO 160
Excited State 1: 2.029-A 1.6377 eV 757.08 nm f=0.0154 <S**2>=0.779
153B ->159B 0.15287
154B ->159B 0.11220
158B ->159B 0.97382
Excited State 2: 2.031-A 1.8441 eV 672.31 nm f=0.0062 <S**2>=0.781
153B ->159B 0.28799
154B ->159B 0.26603
156B ->159B 0.90178
158B ->159B -0.13597
Excited State 3: 2.035-A 1.8828 eV 658.50 nm f=0.0123 <S**2>=0.785
152B ->159B -0.19333
153B ->159B -0.33712
154B ->159B 0.40874
155B ->159B 0.31643
157B ->159B 0.75540
Excited State 4: 2.030-A 1.9233 eV 644.64 nm f=0.0016 <S**2>=0.781
153B ->159B -0.21604
154B ->159B 0.39907
155B ->159B 0.64276
157B ->159B -0.60521
Excited State 5: 2.034-A 2.0457 eV 606.08 nm f=0.0790 <S**2>=0.785
153B ->159B 0.60933
154B ->159B 0.62466
155B ->159B -0.17676
156B ->159B -0.41090
158B ->159B -0.14352
Excited State 6: 2.039-A 2.0599 eV 601.90 nm f=0.1917 <S**2>=0.790
159A ->162A 0.11400
153B ->159B 0.57887
154B ->159B -0.41106
155B ->159B 0.64872
157B ->159B 0.20304

Figure S8. TD-DFT of optimized **^{3Me}a-b** and **^{3Pr}a-b** at the UB3LYP/cc-pVDZ level. Experimental absorption (blue) and Oscillator strength (black).

4.3 Spin density distribution

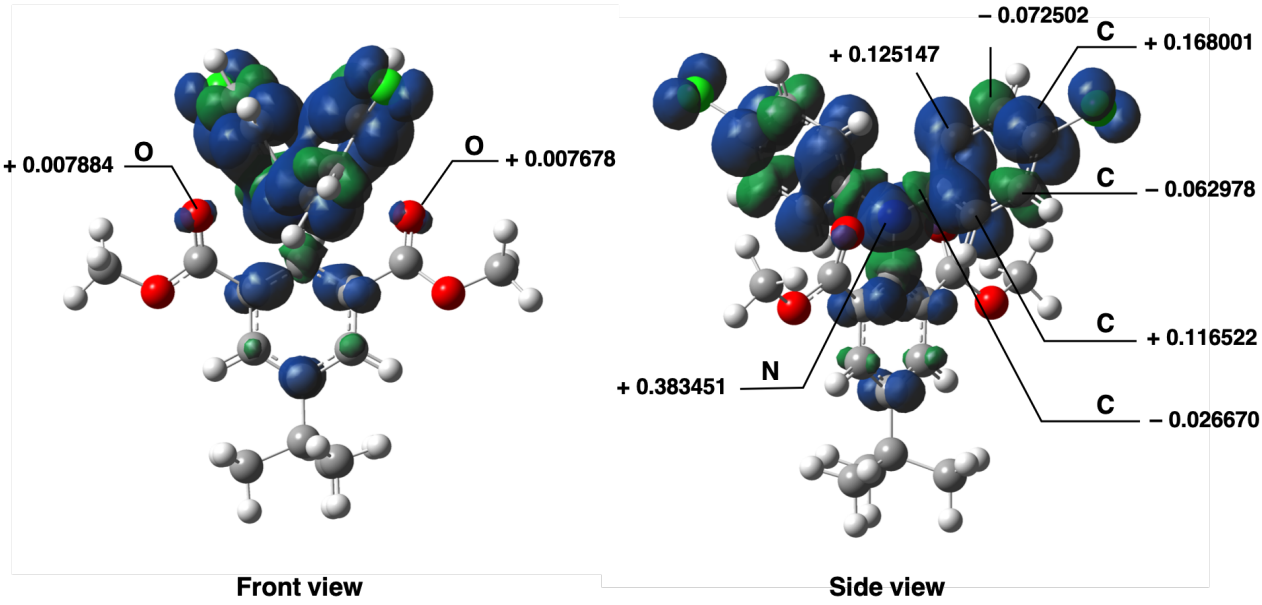

Figure S9. Spin density distribution of the optimized structure of $\mathbf{3^{Me}a}$, calculated at the UB3PW91/6-31G(d) level.

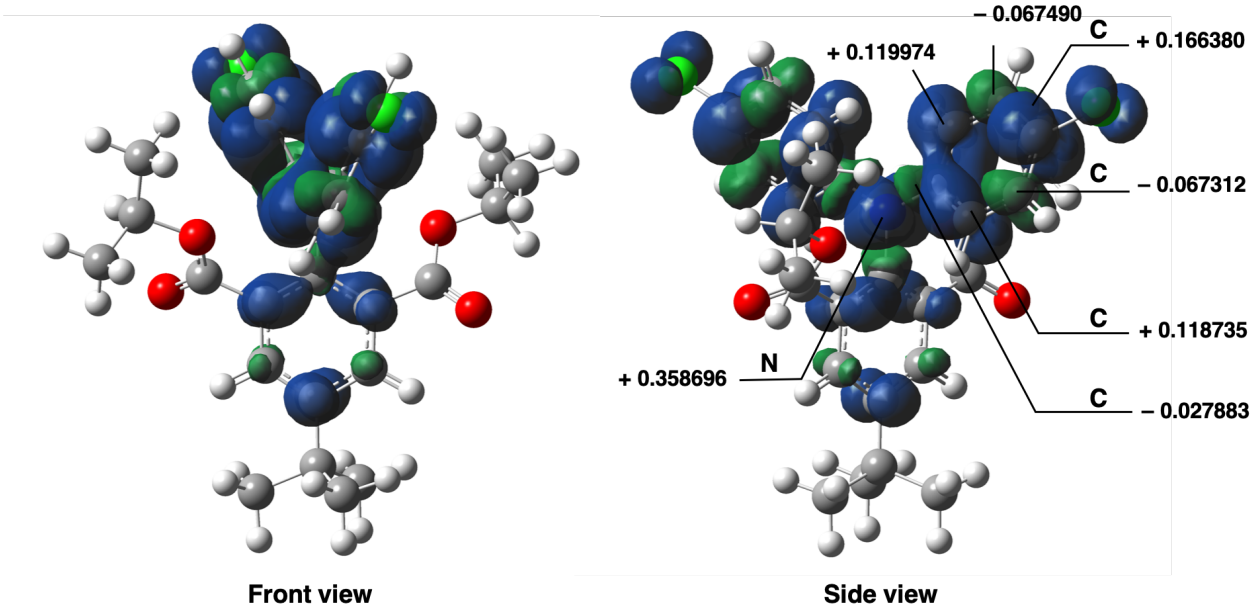

Figure S10. Spin density distribution of the optimized structure of $\mathbf{3^{iPr}a}$, calculated at the UB3PW91/6-31G(d) level.

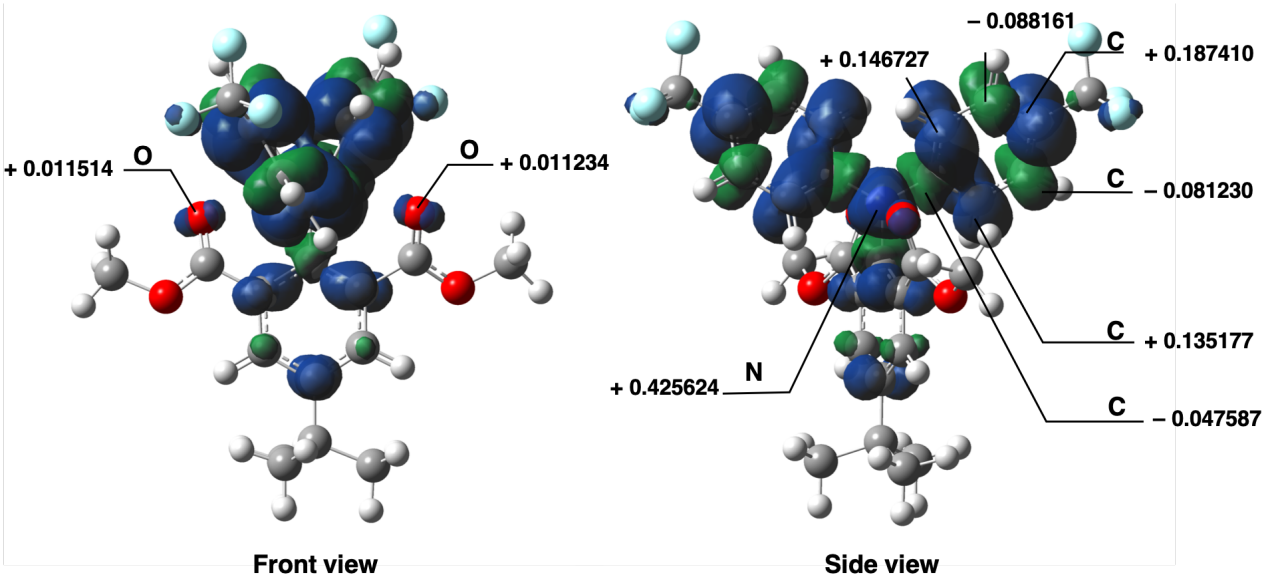

Figure S11. Spin density distribution of the optimized structure of $\mathbf{3^{Me}b}$, calculated at the UB3PW91/6-31G(d) level.

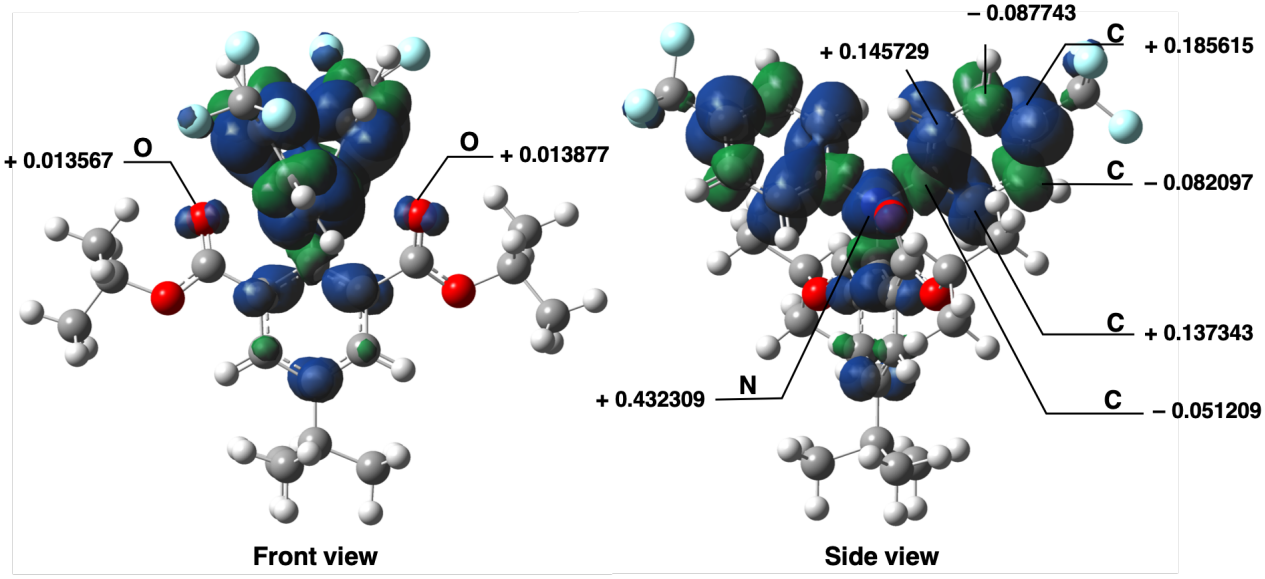

Figure S12. Spin density distribution of the optimized structure of $\mathbf{3^{iPr}b}$, calculated at the UB3PW91/6-31G(d) level.

4.4 The atoms in molecules (AIM)

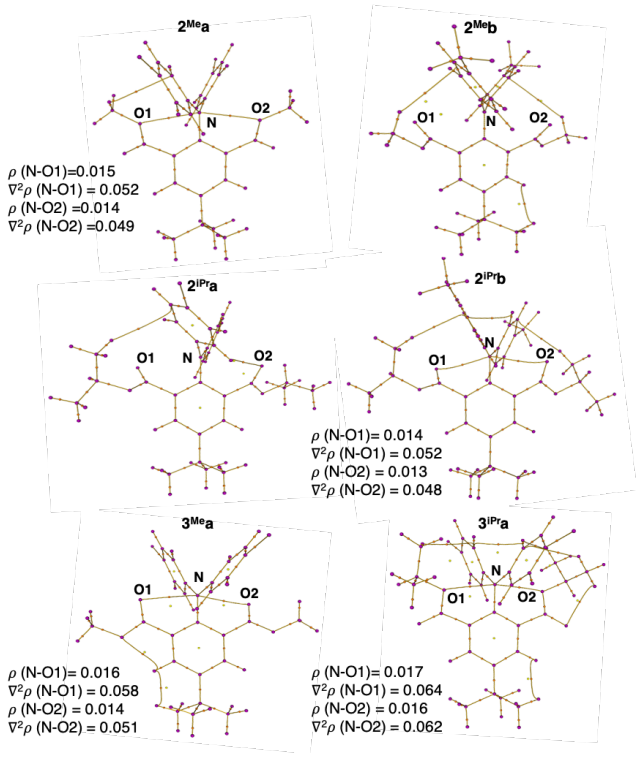

Figure S13. Atom in Molecules (AIM) analysis based on X-ray geometries of **2^{Me}a-b**, **2^{iPr}a-b, 3^{Me}a** and **3^{iPr}a** showing bond paths between the central nitrogen and the carbonyl oxygen, calculated at the RCAM- and UCAM-B3LYP-D3/def2-SVP levels in **2** and **3**, respectively.

Table S10. Summary of the electron density ($\rho(\mathbf{r})$ e/a_o^3), Laplacian ($\nabla^2\rho(\mathbf{r})$ e/a_o^5) at the bond critical point (bcp) of the N-O bonds, and AIM analysis along with kinetic energy density G(r), potential energy density V(r), and energy density H(r) at the (3, –1) critical point in between N and O based on X-ray geometry.

Parameters	Ionic radical	Neutral		Ionic radical	Neutral	
	3^{Me}a	**2^{Me}a**	**2^{Me}b**	**3^{iPr}a**	**2^{iPr}a**	**2^{iPr}b**
Coord.	(C***O***)	(***O***Me)	(C***O***)	(***O***iPr)	(C***O***)	(C***O***)
ρ (N-O1)	0.016029	0.014962	–	0.016690	–	0.013793
$\nabla^2\rho$ (N-O1)	0.058460	0.052404	–	0.064195	–	0.052479
ρ (N-O2)	0.013945	0.013607	–	0.016114	–	0.013087
$\nabla^2\rho$ (N-O2)	0.051214	0.048605	–	0.062402	–	0.048313
V (potential, N-O1)	–0.011815	–0.011446	–	–0.012760	–	–0.010524
G (kinetic, N-O1)	0.013215	0.012274	–	0.014404	–	0.011822
H (total, N-O1)	0.001400	0.000827	–	0.001644	–	0.001298
|V|/G (N-O1)	0.894	0.933	–	0.886	–	0.890
G/ρ (N-O1)	0.824	0.820	–	0.863	–	0.857
H/ρ (N-O1)	0.087	0.055	–	0.099	–	0.094
V (potential, N-O2)	–0.010297	–0.010535	–	–0.012367	–	–0.009938
G (kinetic, N-O2)	0.011550	0.011343	–	0.013984	–	0.011008
H (total, N-O2)	0.001253	0.000808	–	0.001617	–	0.001070
|V|/G (N-O2)	0.892	0.929	–	0.884	–	0.903
G/ρ (N-O2)	0.828	0.868	–	0.868	–	0.841
H/ρ (N-O2)	0.090	0.062	–	0.100	–	0.082

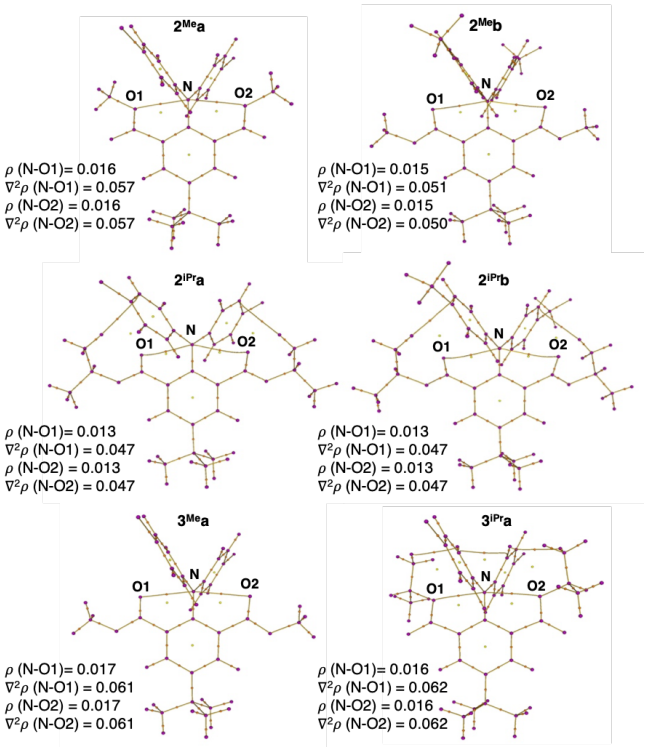

Figure S14. Atom in Molecules (AIM) analysis based on fully optimized geometries of **2^{Me}a-b**, **2^{iPr}a-b, 3^{Me}a** and **3^{iPr}a** showing bond paths between the central nitrogen and the carbonyl oxygen, calculated at the RCAM- and UCAM-B3LYP-D3/def2-SVP levels in **2** and **3**, respectively.

Table S11. Summary of the electron density (ρ(**r**) e/a_o^3), Laplacian ($\nabla^2\rho$(**r**) e/a_o^5) at the bond critical point (bcp) of the N-O bonds, and AIM analysis along with kinetic energy density G(r), potential energy density V(r), and energy density H(r) at the (3, –1) critical point in between N and O based on fully optimized geometry.

Parameters	Ionic radical	Neutral		Ionic radical	Neutral	
	3^{Me}a	**2^{Me}a**	**2^{Me}b**	**3^{iPr}a**	**2^{iPr}a**	**2^{iPr}b**
Coord.	(C***O***)	(***O***Me)	(C***O***)	(***O***iPr)	(C***O***)	(C***O***)
ρ (N-O1)	0.016943	0.015888	0.014791	0.016275	0.012671	0.012714
$\nabla^2\rho$ (N-O1)	0.061432	0.057241	0.050928	0.062634	0.047075	0.047472
ρ (N-O2)	0.016889	0.015873	0.014641	0.016165	0.012601	0.012642
$\nabla^2\rho$ (N-O2)	0.061145	0.057130	0.050375	0.062058	0.047001	0.047369
V (potential)	–0.012547	–0.012277	–0.011199	–0.012377	–0.009665	–0.009629
G (kinetic)	0.013953	0.013280	0.011965	0.013946	0.010717	0.010736
H (total)	0.001405	0.001003	0.000767	0.001569	0.001052	0.001107
|V|/G	0.899	0.924	0.936	0.887	0.902	0.897
G/ρ	0.823	0.837	0.809	0.863	0.846	0.849
H/ρ	0.0829	0.0632	0.0519	0.0971	0.0830	0.0876

Atoms in Molecules (AIM) analysis based on fully optimized geometries of **2^{Me}a-b**, **2^{iPr}a-b, 3^{Me}a** and **3^{iPr}a** showed bond paths between the central nitrogen atom and the ester oxygen atoms in both cation radical and neutral species. The observed 12-N-5 weakly coordinating interaction in neutral compounds may due to the effective delocalization of the lone pair on nitrogen atom and the residue positive charge on nitrogen then can form electrostatic interactions with the adjacent oxygen electron pairs, forming a $n_O \rightarrow \pi^*_{NC}$ interaction as we explained in text.

4.5 The energy difference between sp² carbonyl (C*O*) and alkoxyl (*O*R) coordination modes

Table S12. Single Point (SP) Calcs. at B3LYP-D3/6-31+G* levels for the energy difference between sp² carbonyl (C*O*) and alkoxyl (*O*R) coordination modes. [a,b]

	Carbonyl oxygen [kcal/mol]	Alkoxyl oxygen [kcal/mol]	Difference [kcal/mol]
2^{Me}a	–1431986.818	–1431988.364	1.55
2^{Me}b	–1278208.598	–1278209.961	1.36
2^{iPr}a	–1530690.305	–1530689.352	–0.95
2^{iPr}b	–1376912.023	–1376911.236	–0.79
3^{Me}a	–1431860.742	–1431860.633	–0.11
3^{Me}b	–1278074.77	–1278074.30	–0.47
3^{iPr}a	–1530564.449	–1530562.042	–2.40
3^{iPr}b	–1376778.493	–1376775.592	–2.90

[a] RB3LYP-D3/6-311G* (neutral) and UB3LYP-D3/6-311G* (cationic) levels for geometry optimization and frequency analysis. [b] IEFPCM (CH_2Cl_2 solvent) for solvent effects.

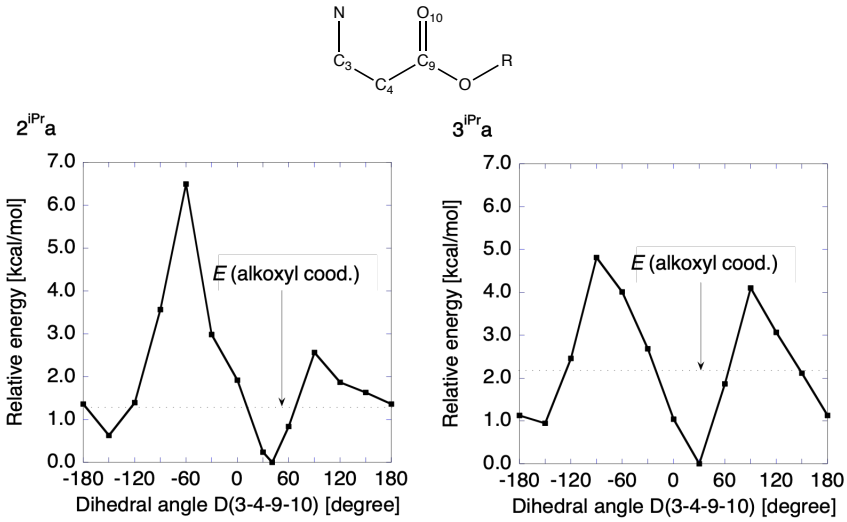

Figure S15. Relaxed potential energy scan for the rotation of *single* COOR group of **2^{iPr}a** and **3^{iPr}a** at the RCAM- and UCAM-B3LYP-D3/def2-SVP levels, respectively. The other COOR group is carbonyl coordination. Vertical axis shows the relative energy E to the total energy at the lowest local minimum structure. Dotted line shows the relative energy for the local minimum where both COOR groups are alkoxyl coordination. Note that X-ray geometries were carbonyl coordination for **2^{iPr}a** and alkoxyl coordination for **3^{iPr}a**, whereas the calculated lowest minimum geometries are predicted to be carbonyl coordination for both systems.

4.6 Examination of applicability of CAM-B3LYP-D3 density for the population and topological analyses

Examination of applicability of CAM-B3LYP-D3 density for the population and topological analyses in comparison with the results from DLPNO-CCSD linearized density by employing simplified models **2x** and **3x**.

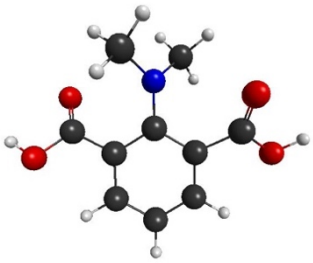

Figure S16. Structure of simplified model **2x**/**3x** (carbonyl coordination).

Table S13. Selected calculated bond lengths (Å), angles and dihedral angles [°] for **2x** and **3x** at the RCAM- and UCAM-B3LYP-D3/def2-SVP levels in **2x** and **3x**, respectively.

Parameters	Ionic radical		Neutral	
	3x	**3x**	**2x**	**2x**
Coord.	(C***O***)	(***O***H)	(C***O***)	(***O***H)
N-O1	2.534	2.644	2.877	2.795
N-O2	2.534	2.644	2.877	2.795
N-C1	1.435	1.408	1.376	1.384
N-C2	1.457	1.452	1.450	1.447
N-C3	1.457	1.452	1.450	1.447
ΣNα	360.0	360.0	360.0	360.0
Φ_{OCCO}	3.2	47.8	59.3	69.31

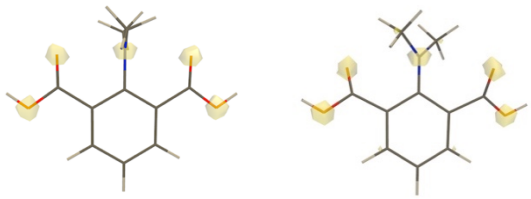

Figure S17. Difference of CAM-B3LYP-D3/def2-SVP density and DLPNO-CCSD/def2-SVP linearized density, ρ(CAM-B3LYP-D3) – ρ(DLPNO-CCSD) (for CO coordination, left: **3x**, right: **2x**:). Yellow/blue surfaces in isosurface maps represent positive and negative region of with contour values of **±0.005** a.u. For ionic radical species, ROHF-DLPNO-CCSD method is employed.

Table S14. Comparison of CAM-B3LYP-D3/def2-SVP and DLPNO-CCSD/def2-SVP (linearized density) results for NPA charges and AIM analysis (for CO coordination).

	Ionic radical **3x**		Neutral **2x**	
	CAM-B3LYP	DLPNO-CCSD	CAM-B3LYP	DLPNO-CCSD
Coord.	(C***O***)	(C***O***)	(C***O***)	(C***O***)
q(N)	-0.087	-0.058	-0.492	-0.488
q(O1)	-0.622	-0.582	-0.621	-0.573
q(O2)	-0.622	-0.582	-0.621	-0.573
q(C1)	0.187	0.163	0.283	0.256
q(C2)	-0.426	-0.381	-0.405	-0.353
q(C3)	-0.426	-0.381	-0.405	-0.353
ρ (N-O1)	0.02220	0.02244	0.01268	0.01303
$\nabla^2\rho$ (N-O1)	0.08266	0.08319	0.04599	0.04687
ρ (N-O2)	0.02219	0.02243	0.01267	0.01303
$\nabla^2\rho$ (N-O2)	0.08261	0.08314	0.04599	0.04687

4.7 The comparison of optimized two electron oxidation species vs optimized one electron oxidation species

We optimized the geometries of two electron oxidized species (**4^{Me}a-b**, **4^{iPr}a-b**). Results are listed in Table S15. In Table S16 and S17, we also listed the results of cationic radical and neutral species. Because of some difficulties in the optimizations, we could not have obtained yet the optimized geometries of **4^{Me}b** (CO) and **4^{iPr}a** (OiPr). Changes in the geometric parameters by oxidization, such as dihedral angle Φ_{OCCO}, are found to be not monotonic. However, some systems of alkoxyl coordination type (**4^{Me}b** and **4^{iPr}b**) are found to have very large dihedral angle of Φ_{OCCO}.

Table S15. Selected calculated bond lengths (Å), angles and dihedral angles [°] for **4^{Me}a-b**, **4^{iPr}a-b** optimized at the RCAM-B3LYP-D3/def2-SVP level.

ParParameters	Dicationic				Dicationic			
	4^{Me}a		**4^{Me}b**		**4^{iPr}a**		**4^{iPr}b**	
Coord.	(C***O***)	(***O***Me)	(C***O***)	(***O***Me)	(C***O***)	(***O***iPr)	(C***O***)	(***O***iPr)
N-O1	2.650	2.676	–[a)]	2.823	2.732	–[a)]	2.848	2.931
N-O2	2.648	2.677	–[a)]	2.813	2.747	–[a)]	2.853	2.901
N-C1	1.438	1.423	–[a)]	1.378	1.420	–[a)]	1.382	1.370
N-C2	1.359	1.364	–[a)]	1.385	1.365	–[a)]	1.382	1.389
N-C3	1.359	1.364	–[a)]	1.386	1.364	–[a)]	1.381	1.390
ΣNα	360.0	360.0	–[a)]	360.0	360.0	–[a)]	360.0	360.0
Φ_{OCCO}	37.4	62.7	–[a)]	91.3	60.5	–[a)]	72.3	98.8

[a)] Geometry optimization has not been completed primarily due to the difficulty of convergence.

Table S16. Selected calculated bond lengths (Å), angles and dihedral angles [°] for **3^{Me}a** and **3^{iPr}a** at the UCAM-B3LYP-D3/def2-SVP level.

ParParameters	Cationic radical				Cationic radical			
	3^{Me}a		**3^{Me}b**		**3^{iPr}a**		**3^{iPr}b**	
Coord.	(C***O***)	(***O***Me)	(C***O***)	(***O***Me)	(C***O***)	(***O***iPr)	(C***O***)	(***O***iPr)
N-O1	2.686	2.654	–[a)]	2.652	2.732	2.676	2.787	–[a)]
N-O2	2.684	2.656	–[a)]	2.654	2.731	2.673	2.788	–[a)]
N-C1	1.435	1.434	–[a)]	1.433	1.431	1.439	1.424	–[a)]
N-C2	1.388	1.388	–[a)]	1.390	1.388	1.388	1.393	–[a)]
N-C3	1.387	1.388	–[a)]	1.390	1.388	1.387	1.393	–[a)]
ΣNα	360.0	360.0	–[a)]	360.0	360.0	360.0	360.0	–[a)]
Φ_{OCCO}	39.1	54.1	–[a)]	55.2	57.4	47.0	66.4	–[a)]

[a)] Geometry optimization has not been completed primarily due to the difficulty of convergence.

Table S17. Selected calculated bond lengths (Å), angles and dihedral angles [°] for **2^{Me}a** and **2^{iPr}a** at the RCAM-B3LYP-D3/def2-SVP level.

ParParameters	Neutral				Neutral			
	2^{Me}a		**2^{Me}b**		**2^{iPr}a**		**2^{iPr}b**	
Coord.	(C***O***)	(***O***Me)	(C***O***)	(***O***Me)	(C***O***)	(***O***iPr)	(C***O***)	(***O***iPr)
N-O1	2.826	2.734	2.795	–[a)]	2.885	2.747	2.882	2.729
N-O2	2.824	2.734	2.802	–[a)]	2.889	2.806	2.886	2.796
N-C1	1.416	1.417	1.420	–[a)]	1.416	1.422	1.419	1.425
N-C2	1.405	1.405	1.403	–[a)]	1.408	1.398	1.405	1.394
N-C3	1.405	1.405	1.401	–[a)]	1.407	1.413	1.404	1.413
ΣNα	360.0	360.0	360.0	–[a)]	360.0	359.9	360.0	360.0
Φ_{OCCO}	61.4	67.2	56.3	–[a)]	73.6	75.0	74.4	71.3

[a)] Geometry optimization has not been completed primarily due to the difficulty of convergence.

We have also performed the AIM analysis for the (3, –1) critical point of the two-electron oxidized species (Figure S18; experimentally two-electron oxidation is not possible, *cf.* CV data). Please note that, as mentioned in the previous reply, we could not obtain the optimized geometries of **4^{Me}b** (CO) and **4^{iPr}a** (OiPr) despite of much effort.

We have found that for **4^{Me}b** (***O***Me), **4^{iPr}b** (C***O***) and **4^{iPr}b** (***O***iPr), (3, –1) critical points between N and O could not be obtained, whereas those between C and O atoms were obtained. These results indicate that the weak attractive interaction between N atom and O atom may not be observed even in their corresponding dication diradical species (10-N-5), which are considered to have 3-center-4-electron hypervalent bond. In Table S18, we summarized several important values obtained from the AIM analysis.

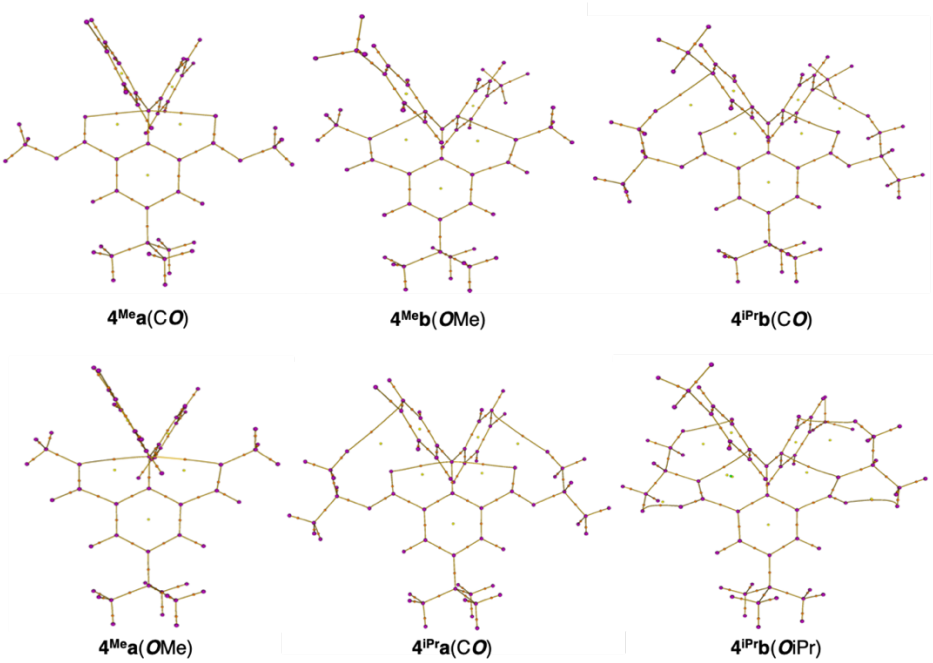

Figure S18. Atom in Molecules (AIM) analysis of **4^{Me}a-b** and **4^{iPr}a-b** calculated at the RCAM -B3LYP-D3/def2-SVP levels.

Table S18. Summary of AIM analysis along with kinetic energy density G(r), potential energy density V(r), and energy density H(r) at the (3, –1) critical point in between O1 and X (X = N or C) for two electron oxidized species.

Parameters	Dicationic				Dicationic			
	4^{Me}a		**4^{Me}b**		**4^{iPr}a**		**4^{iPr}b**	
Coord.	(C***O***)	(***O***Me)	(C***O***)	(***O***Me)[b]	(C***O***)	(***O***iPr)	(C***O***)[b]	(***O***iPr)[b]
ρ (X-O1)	0.017838	0.016007	–[a]	0.014827	0.015295	–[a]	0.014249	0.011407
$\nabla^2\rho$ (X-O1)	0.066352	0.063469	–[a]	0.051968	0.057455	–[a]	0.050160	0.040642
V (potential)	–0.013053	–0.012153	–[a]	–0.010821	–0.011129	–[a]	–0.010070	–0.007783
G (kinetic)	0.014820	0.014010	–[a]	0.011906	0.012747	–[a]	0.011305	0.008972
H (total)	0.001767	0.001857	–[a]	0.001086	0.001617	–[a]	0.001235	0.001189
|V|/G	0.881	0.867	–[a]	0.736	0.873	–[a]	0.891	0.867
G/ρ	0.831	0.875	–[a]	0.803	0.833	–[a]	0.793	0.787
H/ρ	0.0991	0.116	–[a]	0.0732	0.106	–[a]	0.0867	0.104

[a] Geometry optimization has not been completed primarily due to the difficulty of convergence.
[b] Results of (3, -1) critical point in between O1 and C.

5.π-donating methoxy derivative (2^{Me}c)

During revision, in response to reviewers' suggestions on the N-O interactions, we have carried out additional experimental work to synthesize the neutral π-donating methoxy derivative (**2^{Me}c**) as a comparison in addition to the electron-withdrawing substituted derivatives reported in the MS. Since our aim was to enforce the hypervalent bonding (in the 11-N-5 radical cations), we had only electron-withdrawing substituents on the aryl groups initially. AIM on N-O (3, –1) critical points were analyzed based on optimized geometry (Figure S14, Table S11) as well as solid-state geometries (single point calculations based on X-ray structures, Figure 3 and Table 10).

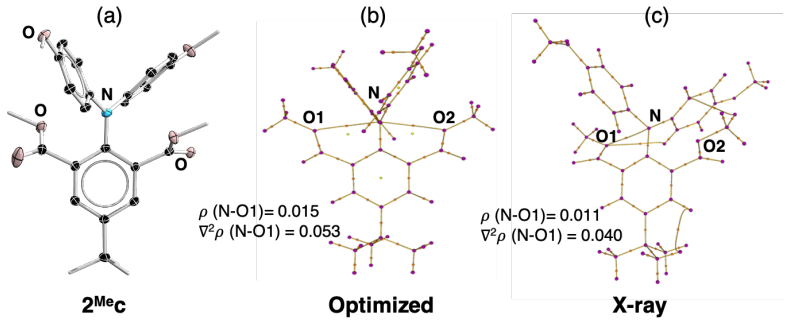

Figure S19. (a) Solid-state molecular structures of **2^{Me}c**. Thermal ellipsoids are set at 30% probability. Ellipsoids of periphery atoms, hydrogen atoms, and counter ions are omitted for clarity. CCDC number: 1988910. (b) AIM analysis of **2^{Me}c** based on optimized geometry. (c) AIM analysis of **2^{Me}c** based on X-ray geometry.

Table S19. Selected experimental and calculated bond lengths (Å), angles, dihedral angles at the RCAM-B3LYP-D3/def2-SVP level of **2^{Me}c** and its summary of AIM analysis along with kinetic energy density G(r), potential energy density V(r), and energy density H(r) at the (3, -1) critical point in between O1 and N.

Parameters	**2^{Me}c**	
	optimized	**X-ray**
Coord.	(***O***Me)	(***O***Me)
N-O1	2.765	2.939(2)
N-O2	2.767	3.051(19)
N-O$_{Ave}$	2.766	2.995(19)
N-C1	1.411	1.410(2)
N-C2	1.410	1.415(2)
N-C3	1.410	1.425(2)
ΣNα	360.0	359.9(38)
Φ_{OCCO}	73.94	112.8
ρ (N-O1)	0.014966	0.010913
$\nabla^2\rho$ (N-O1)	0.053428	0.039661
V (potential)	–0.011569	–0.008410
G (kinetic)	0.012463	0.009163
H (total)	0.000894	0.000752
|V|/G	0.928	0.917
G/ρ	0.833	0.840
H/ρ	0.0597	0.0689

The *optimized* structures significantly underestimate the N-O distances for **2^{Me}b** and **2^{Me}c**, showing the N-O (3, –1) critical points on both sides in all neutral and cationic radical structures (Figures S14 and S19). In contrast, the AIM analysis based on *solid-state structures* showed both N-O (3, –1) critical points in cationic radical species and two of the neutral amines

(**2^{Me}a** and **2^{iPr}b**). These structures also exhibit shorter N-O distances than **2^{Me}b**, **2^{Me}c** and **2^{iPr}a**. The latter structures showed no or only one (3, –1) critical point. The AIM based on X-ray solid-state structures are more reflective than the optimized structures, as the latter are based on significantly shorter N-O distances. The longer N-O distances observed in the solid-state structures are likely due to crystal-packing effect, which means if any N-O attractive interaction exists, it is weaker than crystal-packing effect. Overall, these results suggest that the N-O interactions may not exit in all neutral amine species and if they do, they are very weak.

In addition, comparing the *para*-Cl (**2^{Me}a**) and *para*-OMe (**2^{Me}c**) with same N-O coordination modes, the π-donating OMe derivative showed significantly longer N-O distances and weaker N-O interaction on only one side. However, since we cannot determine how much crystal packing effect contribute to the solid-state structure, we cannot conclude on the OMe π-donating effect on the $n_O \rightarrow p^*_{NC}$ stabilization, which was the original target reason for synthesizing *para*-OMe (**2^{Me}c**). Therefore, the results on **2^{Me}c** is not reported in the MS but in ESI only.

Synthesis of dimethyl 2-(bis(4-methoxyphenyl) amino)-5-(*tert*-butyl) isophthalate (2^{Me}c)

Bis(4-methoxyphenyl) amine (700 mg, 3.03 mmol) was coupled with dimethyl 2-bromo-5-*tert*-butyl-isophthalate (**1^{Me}**) (1.0 g, 3.03 mmol) according to the above Ullmann procedure (19 mL of *n*-Bu_2O) for 96 h at 145 °C. The crude product was purified by flash chromatography using a 1:10 solution of ethyl acetate / hexane as the eluent to give 462 mg (0.968 mmol,32% yield) of the title compound as a yellow solid. ^{1}H NMR (400 MHz, $CDCl_3$) δ (ppm) δ 7.69 (s, 2H), 6.88 (d, J = 8.0 Hz, 4H), 6.74 (s, 4H), 3.74 (s, 6H), 3.50 (s, 6H), 1.33 (s, 9H). ^{13}C NMR (100 MHz, $CDCl_3$) δ (ppm) δ 168.5, 154.8, 147.7, 142.4, 141.3, 131.6, 130.8, 123.5, 114.2, 55.5, 52.2, 34.7, 31.2. MS(ESI) m/z $[M+Na]^+$ $C_{28}H_{31}O_6NNa$ Calcd for: 500.20436 Found: 500.20422. Elemental analysis: Calcld.: C, 70.42; H, 6.54; N, 2.93; Found: C, 70.10; H, 6.24; N, 2.72. M.P.: 94.3-95.4 °C. Crystal data:Formula: $C_{28}H_{31}NO_6$; Mol wt: 477.54; Crystal system: Monoclinic; Space group: $P2_1/c$; *a*, Å: 10.3036(6); *b*, Å: 18.9257(11); *c*, Å: 13.0352(7); *α*, deg: 90; *β*, deg: 94.843(2); *γ*, deg: 90; V, Å^3: 2532.8(2); Z: 4; D_{calc}, Mg/m^3: 1.252; Abs coeff, mm^{-1}: 0.088; *F*(000): 1016; Temp, K:173(2); Reflections:26160; Independent: 5792; *R*int: 0.0463; Parameters: 323; *R1* [$I > 2\sigma(I)$]: 0.0510; wR_2 (all data): 0.1593.

6. NMR spectra

2-Bromo-5-*tert*-butyl-1,3-dimethylbenzene (b)

^{1}H NMR (400 MHz, $CDCl_3$) δ (ppm) 7.11 (s, 2H), 2.43 (s, 6H), 1.31 (s, 9H).

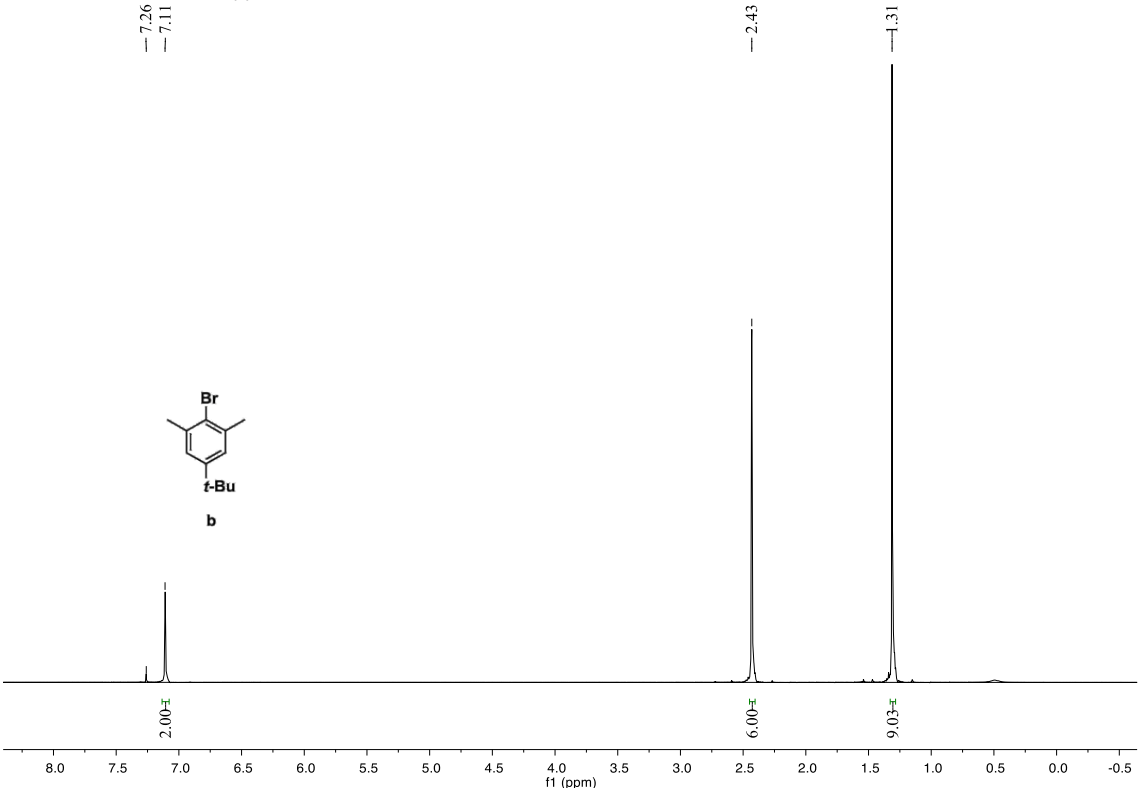

^{13}C NMR (100 MHz, $CDCl_3$) δ (ppm) 149.8, 137.8, 125.6, 124.6, 34.3, 31.4, 24.2.

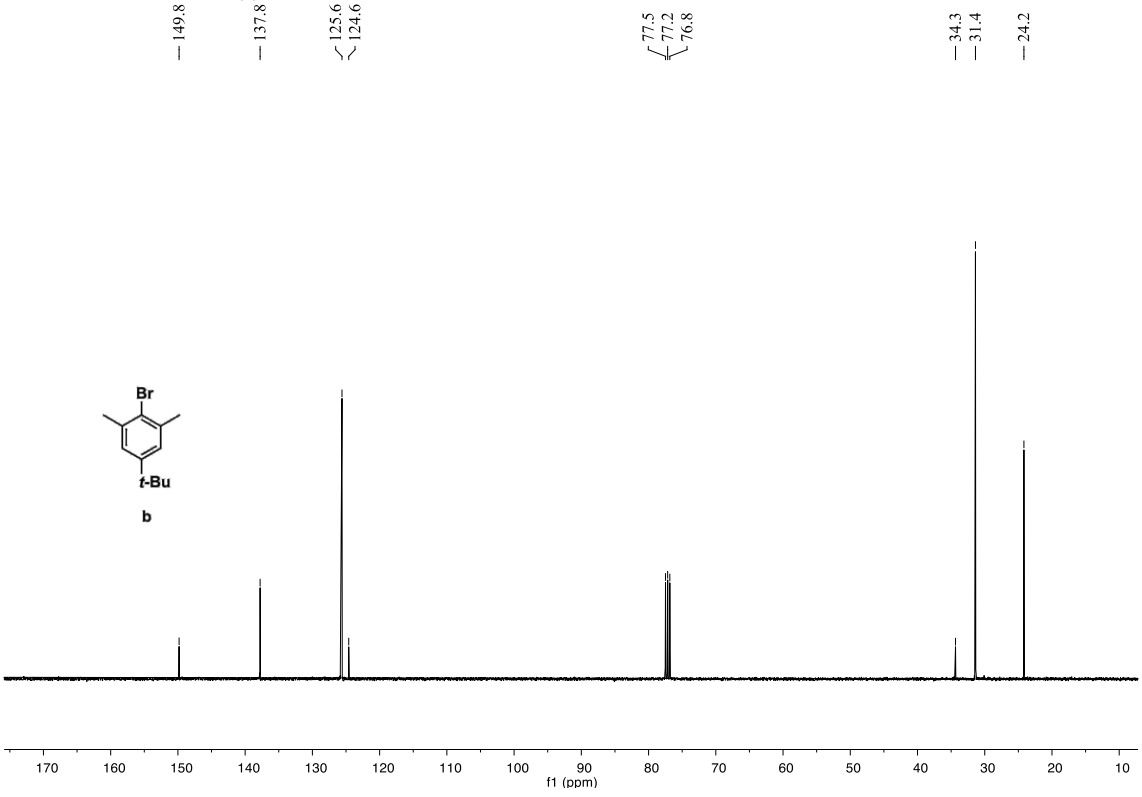

2-Bromo-5-*tert*-butyl-isophthalic Acid (c)

^{1}H NMR (400 MHz, DMSO) δ (ppm) 13.60 (s, 2H), 7.68 (s, 2H), 1.28 (s, 9H).

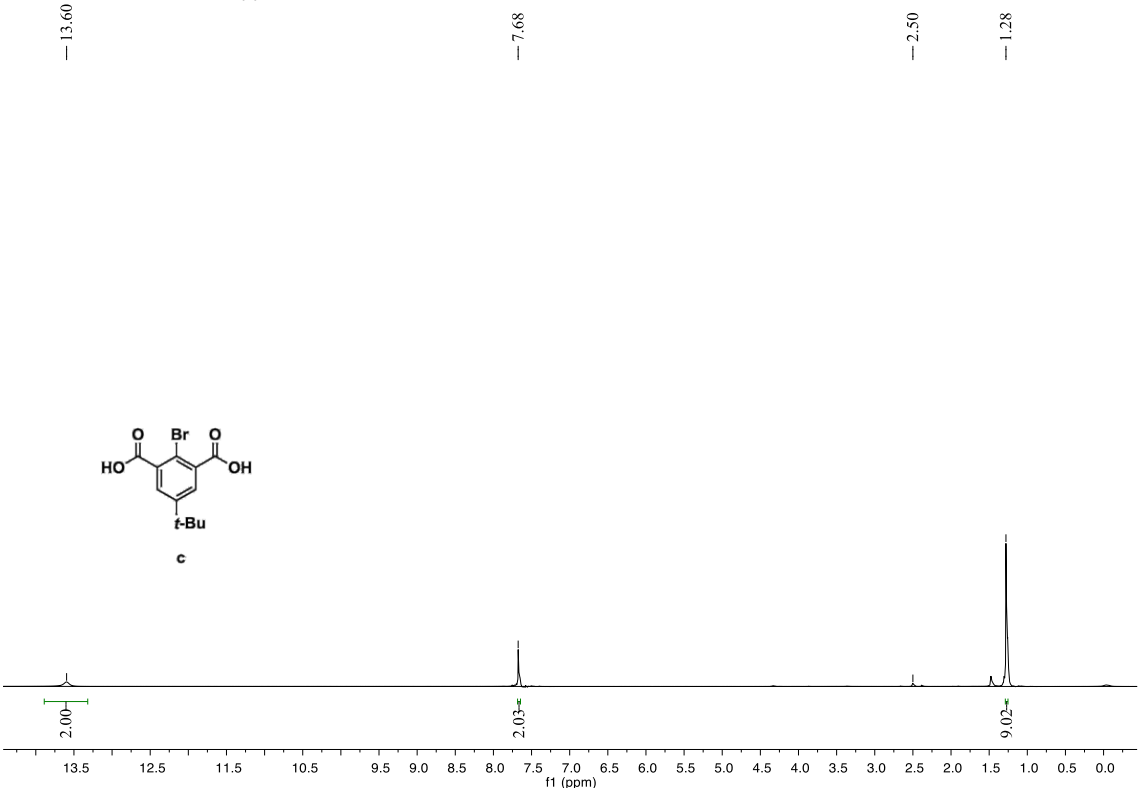

^{13}C NMR (100 MHz, DMSO) δ (ppm) 168.3, 150.7, 136.6, 127.8, 113.3, 34.6, 30.6.

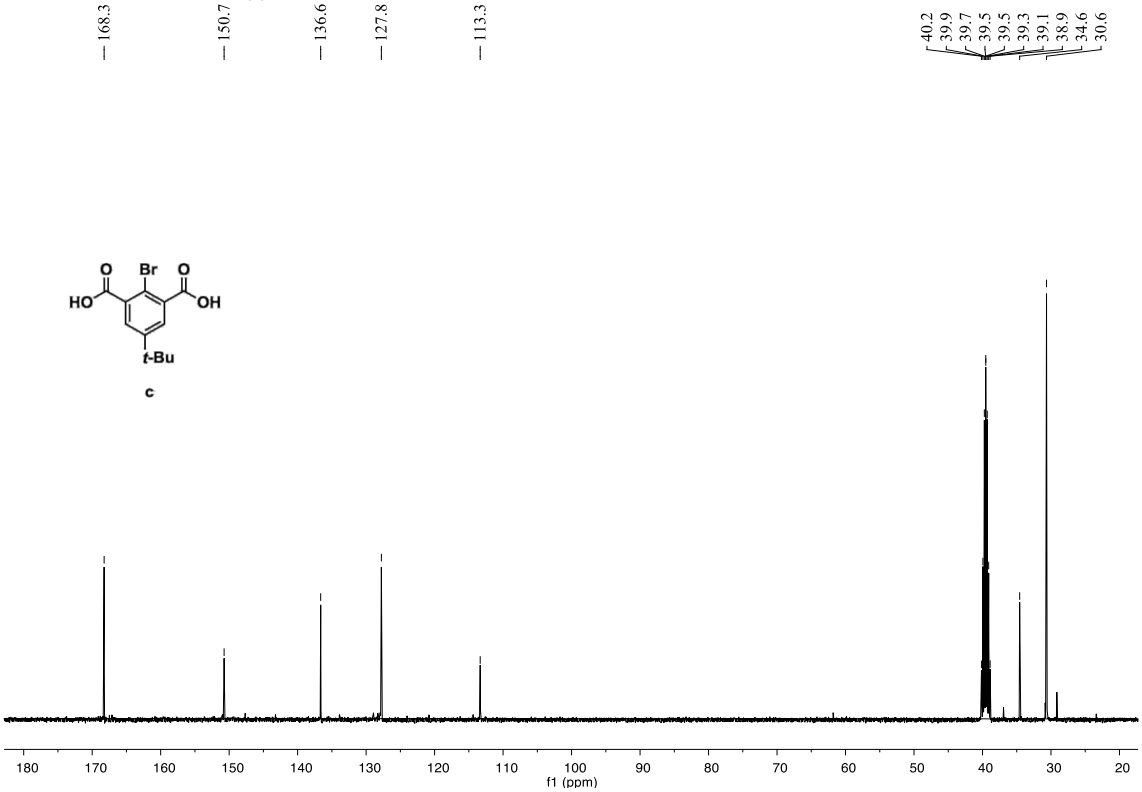

Dimethyl 2-Bromo-5-*tert*-butyl-isophthalate (1^{Me})

^{1}H NMR (400 MHz, $CDCl_3$) δ (ppm) 7.68 (s, 2H), 3.93 (s, 6H), 1.30 (s, 9H).

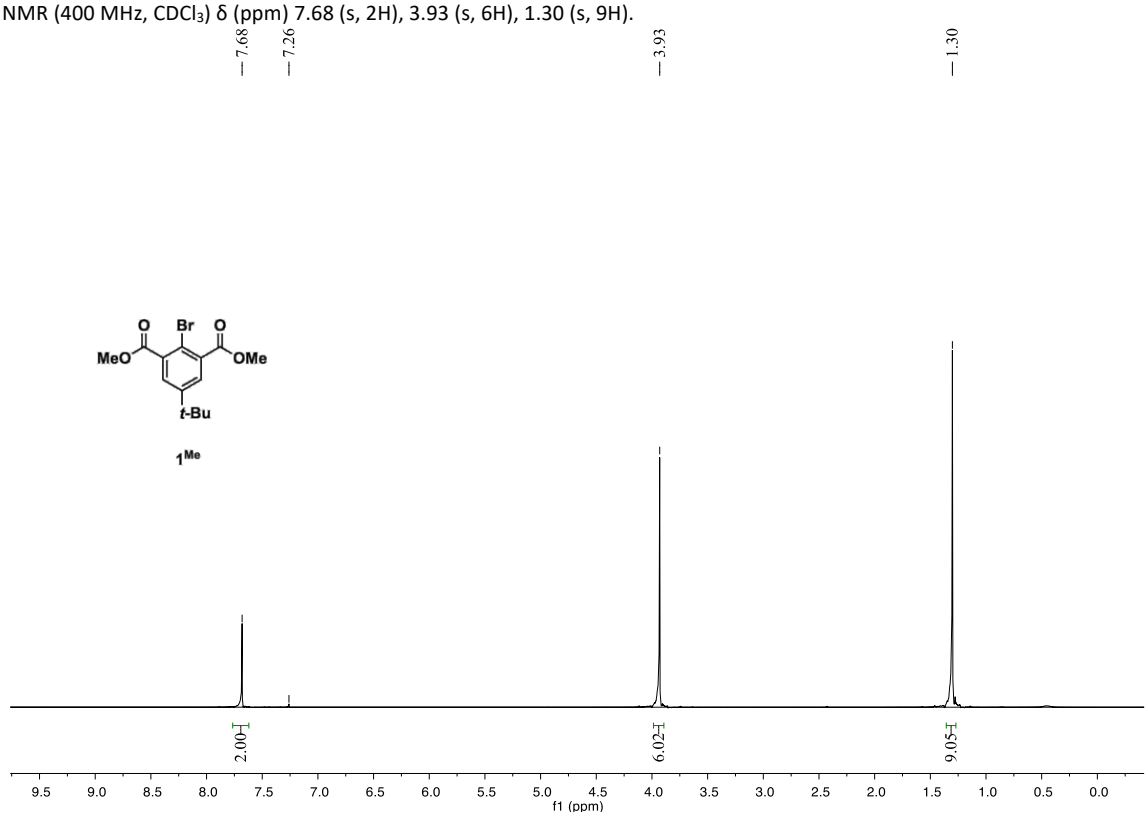

^{13}C NMR (100 MHz, $CDCl_3$) δ (ppm) 167.6, 150.9, 135.1, 129.6, 115.8, 77.48, 52.8, 34.8, 34.0.

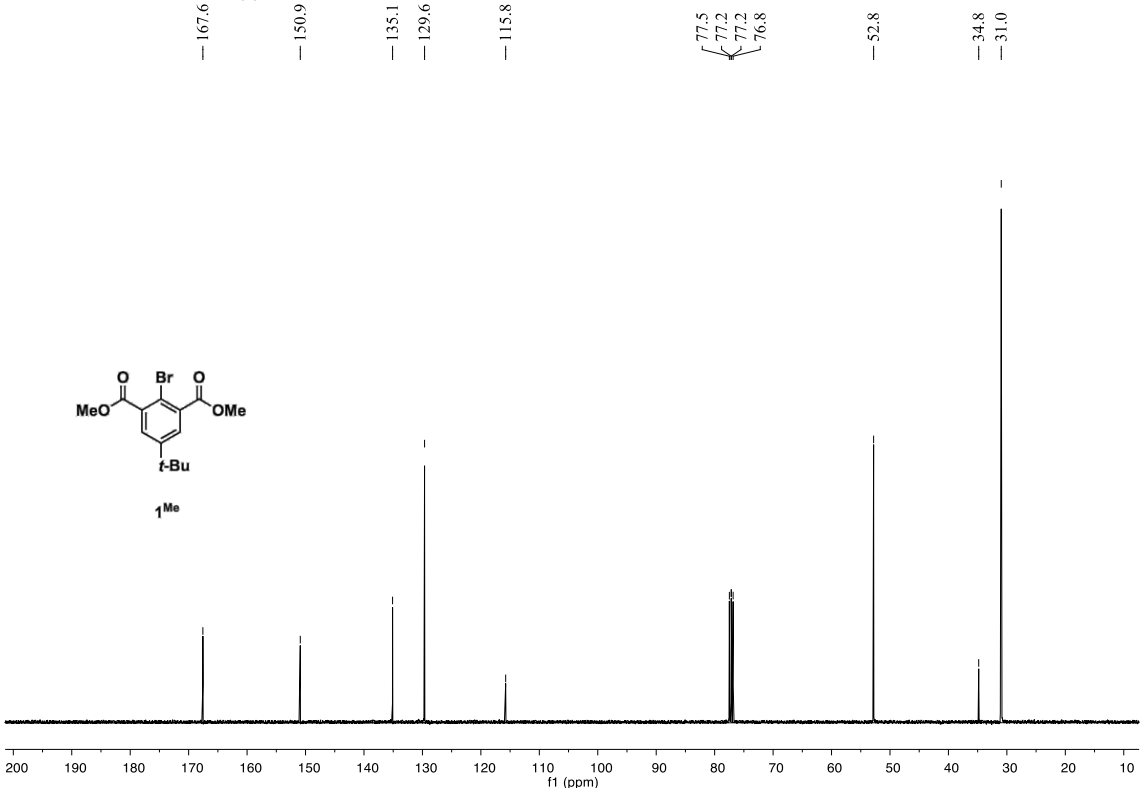

Diisopropyl 2-bromo-5-(*tert*-butyl) isophthalate (1^{iPr})

^{1}H NMR (400 MHz, $CDCl_3$) δ (ppm) 7.59 (s, 2H), 5.32 – 5.22 (m, 2H), 1.38 (d, *J* = 4 Hz, 12H), 1.30 (s, 9H).

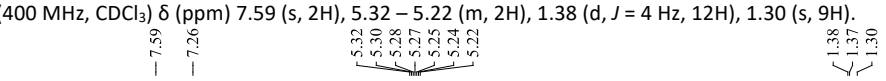

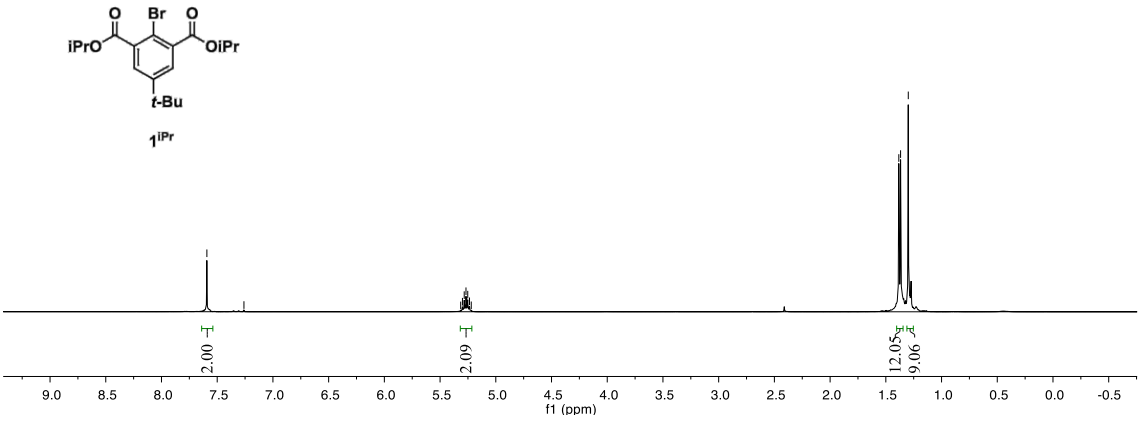

^{13}C NMR (100 MHz, $CDCl_3$) δ (ppm) 166.9, 150.8, 135.9, 128.9, 115.0, 70.0, 34.8, 30.9 21.8.

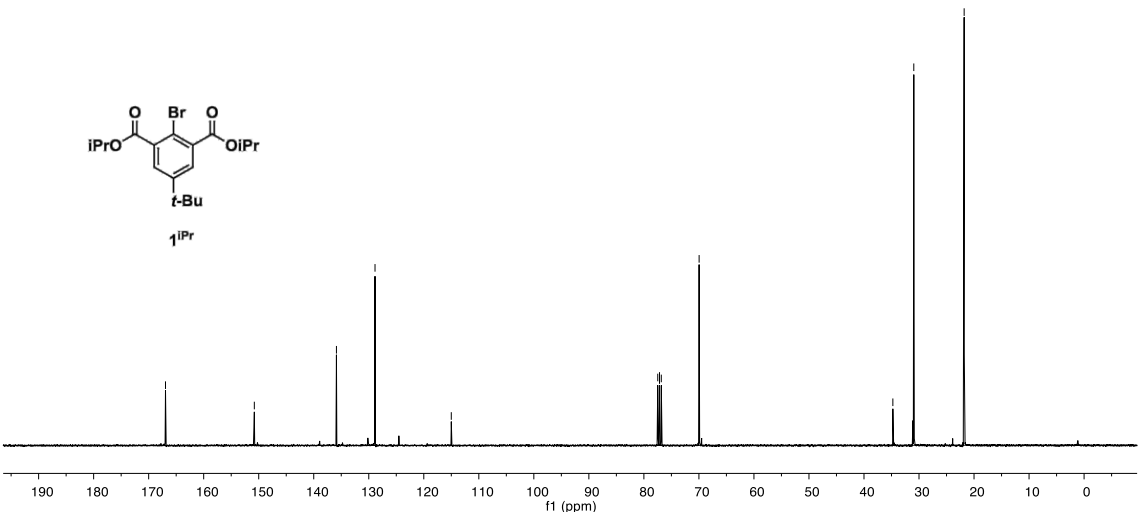

Dimethyl 2-(bis(4-chlorophenyl) amino)-5-(tert-butyl) isophthalate (2^{Me}a)

^{1}H NMR (400 MHz, $CDCl_3$) δ (ppm) 7.81 (s, 2H), 7.14 (d, J = 4 Hz, 4H), 6.87 (d, J = 4 Hz, 4H), 3.54 (s, 6H), 1.36 (s, 9H).

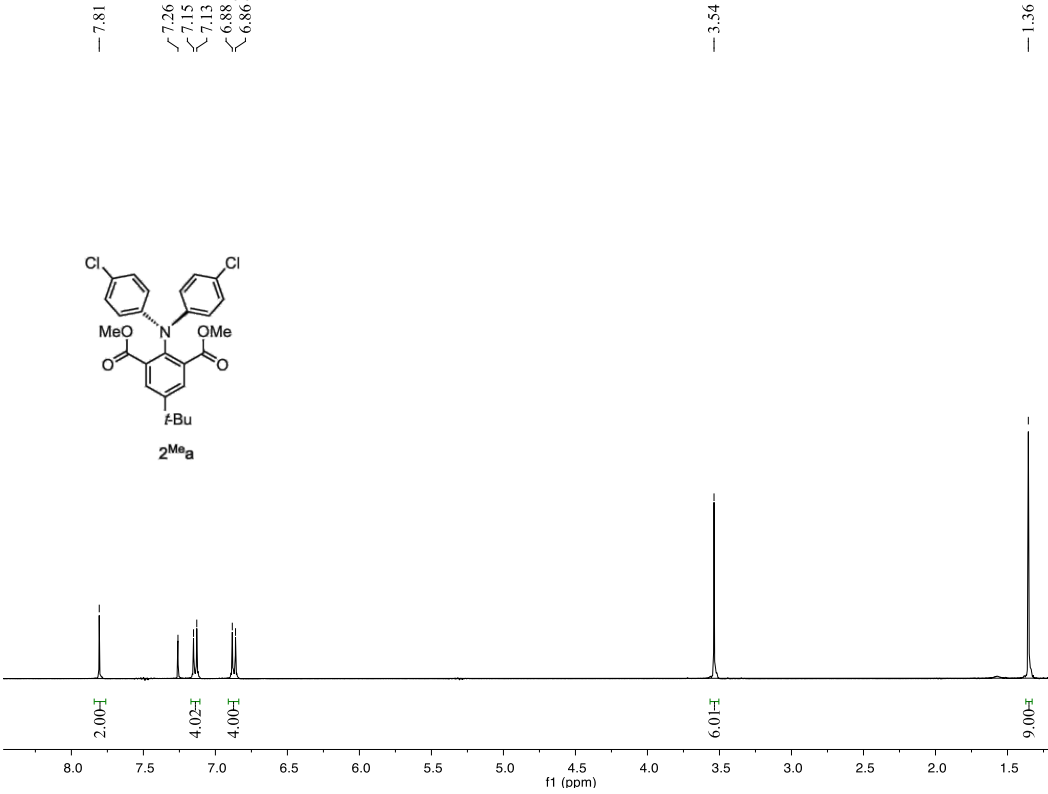

^{13}C NMR (100 MHz, $CDCl_3$) δ (ppm) 167.6, 149.8, 145.5, 141.1, 132.1, 131.4, 129.1, 127.3, 123.3, 52.5, 35.0, 31.2.

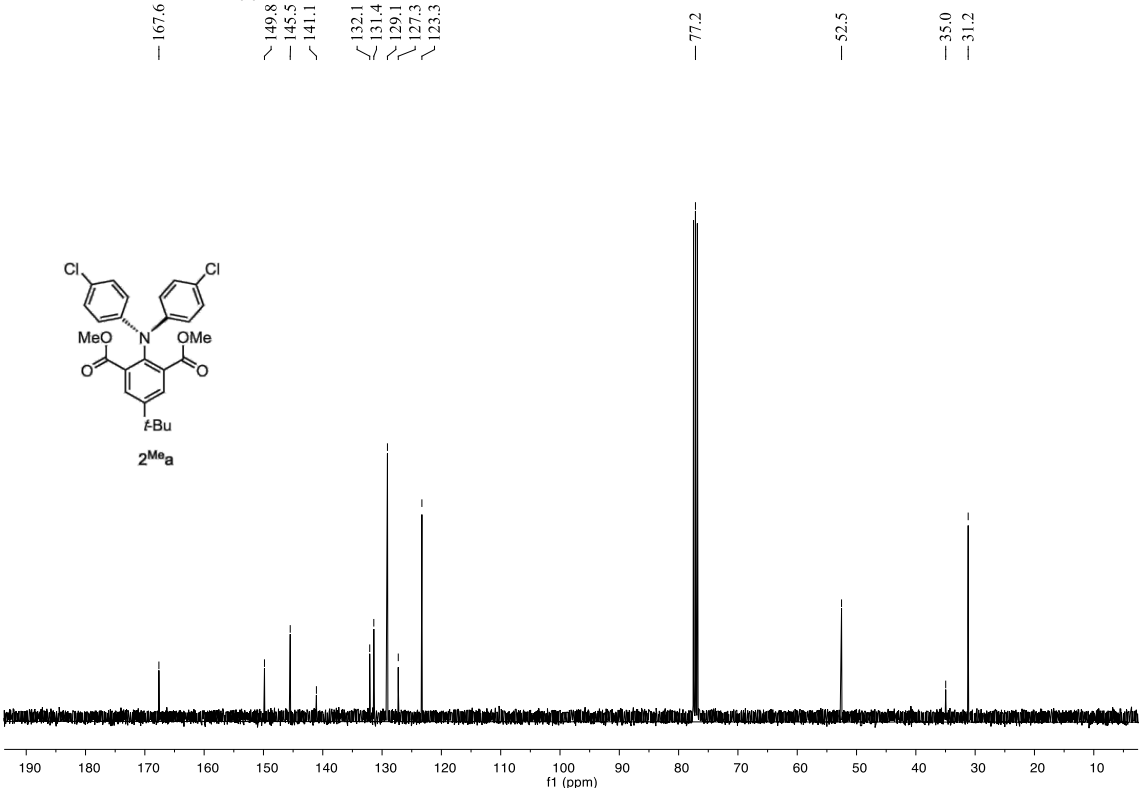

Dimethyl 2-(bis(4-(trifluoromethyl) phenyl) amino)-5-(tert-butyl) isophthalate (2^{Me}b)

^{1}H NMR (400 MHz, $CDCl_3$) δ (ppm) 7.91 (s, 2H), 7.45 (d, *J* = 8 Hz, 4H), 7.04 (d, *J* = 8 Hz, 4H), 3.53 (s, 6H), 1.38 (s, 9H).

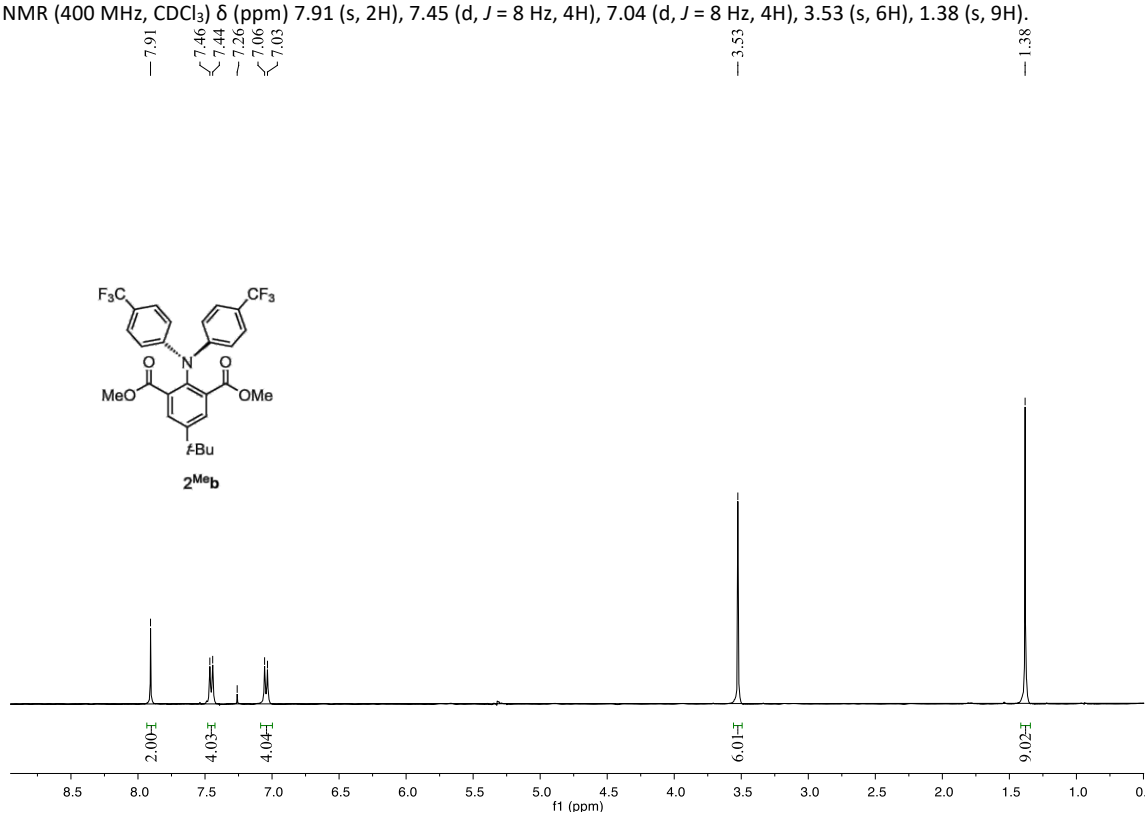

^{13}C NMR (100 MHz, $CDCl_3$) δ (ppm) 167.1, 151.0, 149.2, 140.4, 132.3, 131.7, 126.3 (q, $^{3}J_{C\text{-}F}$ = 10 Hz), 124.4 (q, $^{1}J_{C\text{-}F}$ = 270 Hz), 124.3 (q, $^{2}J_{C\text{-}F}$ = 30 Hz), 121.7, 52.6, 35.1, 31.1.

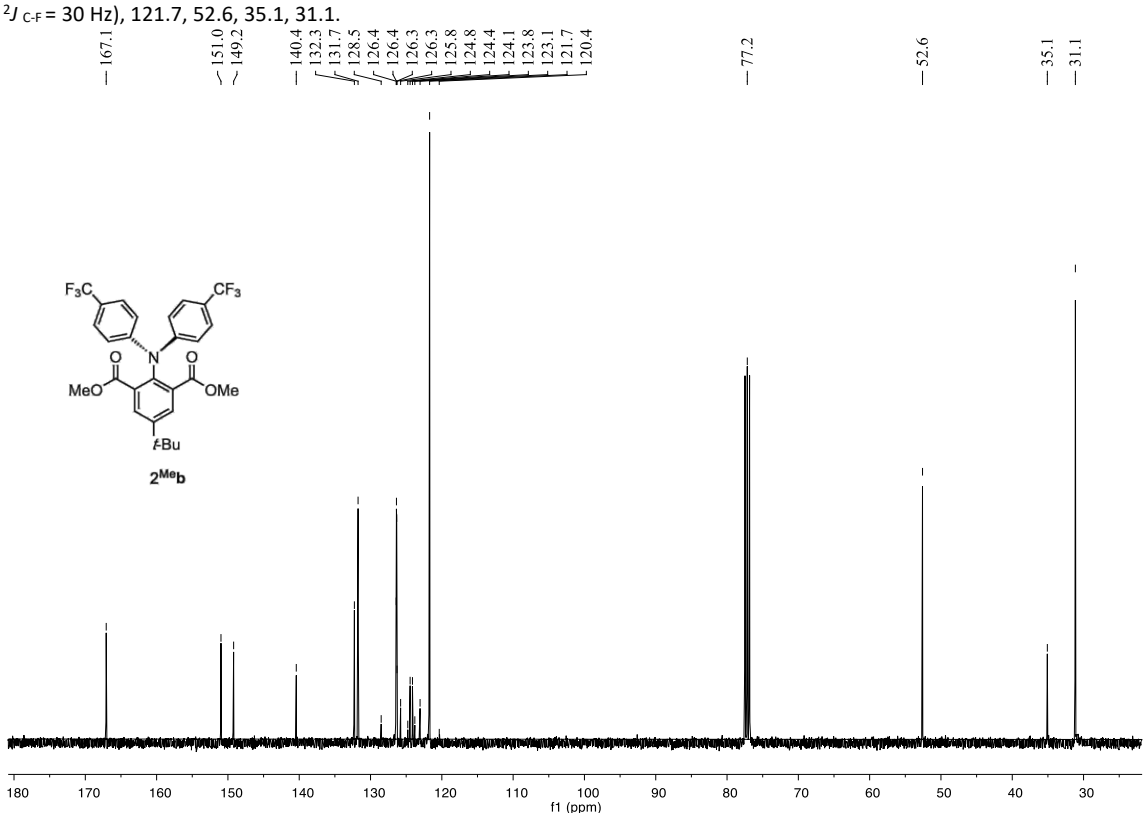

^{19}F NMR (376 MHz, $CDCl_3$) δ (ppm) -62.29.

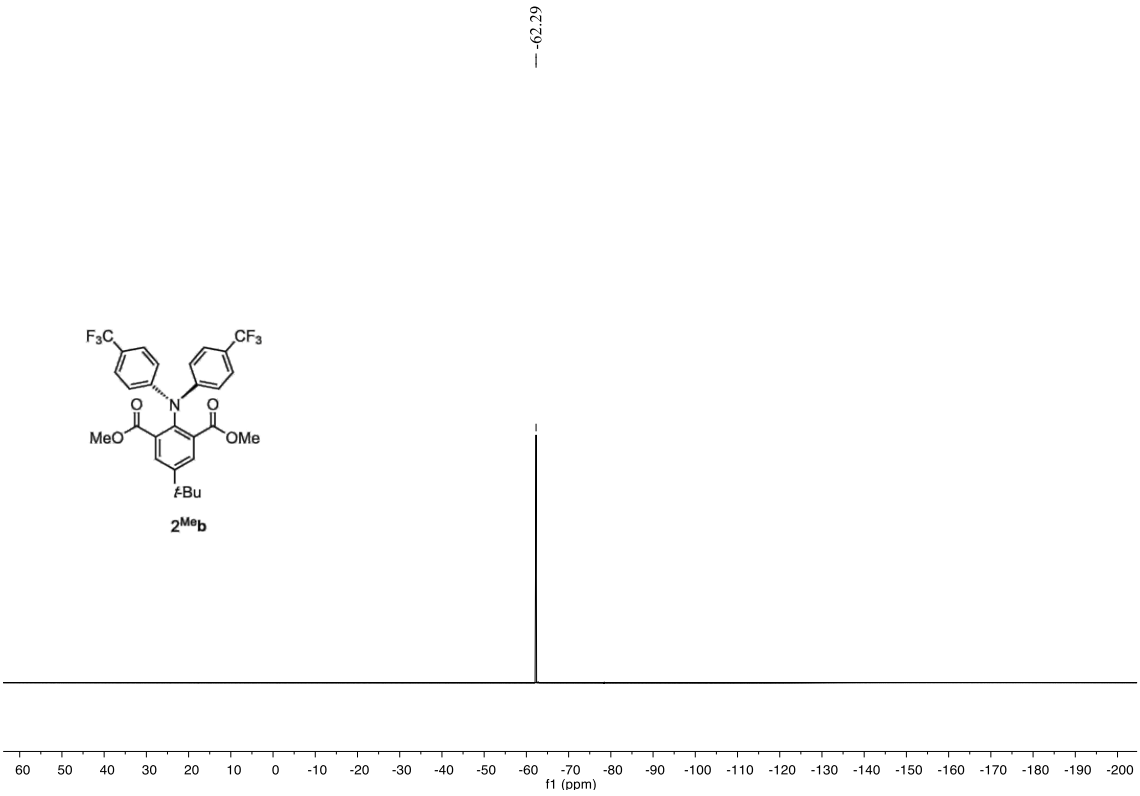

Diisopropyl 2-(bis(4-chlorophenyl) amino)-5-(tert-butyl) isophthalate (2^{iPr}a)

^{1}H NMR (400MHz, $CDCl_3$) δ (ppm) 7.73 (s, 2H), 7.12 (d, *J* = 8 Hz, 4H), 6.90 (d, *J* = 8 Hz, 4H), 4.85 (m, 2H), 1.36 (s, 9H), 1.04 (d, *J* =8 Hz, 12H).

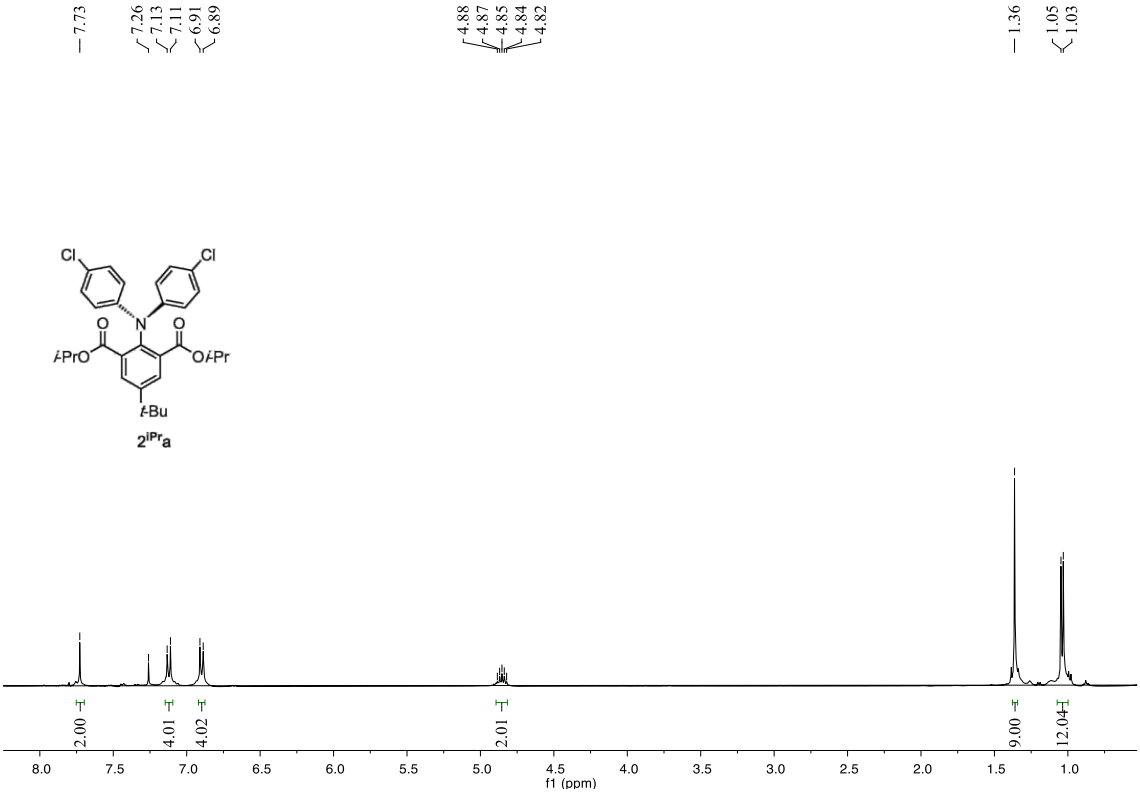

^{13}C NMR (100 MHz, $CDCl_3$) δ (ppm) 166.5, 149.9, 145.3, 140.6, 133.4, 130.4, 128.9, 126.9, 123.1, 69.5, 34.9, 31.2, 21.6.

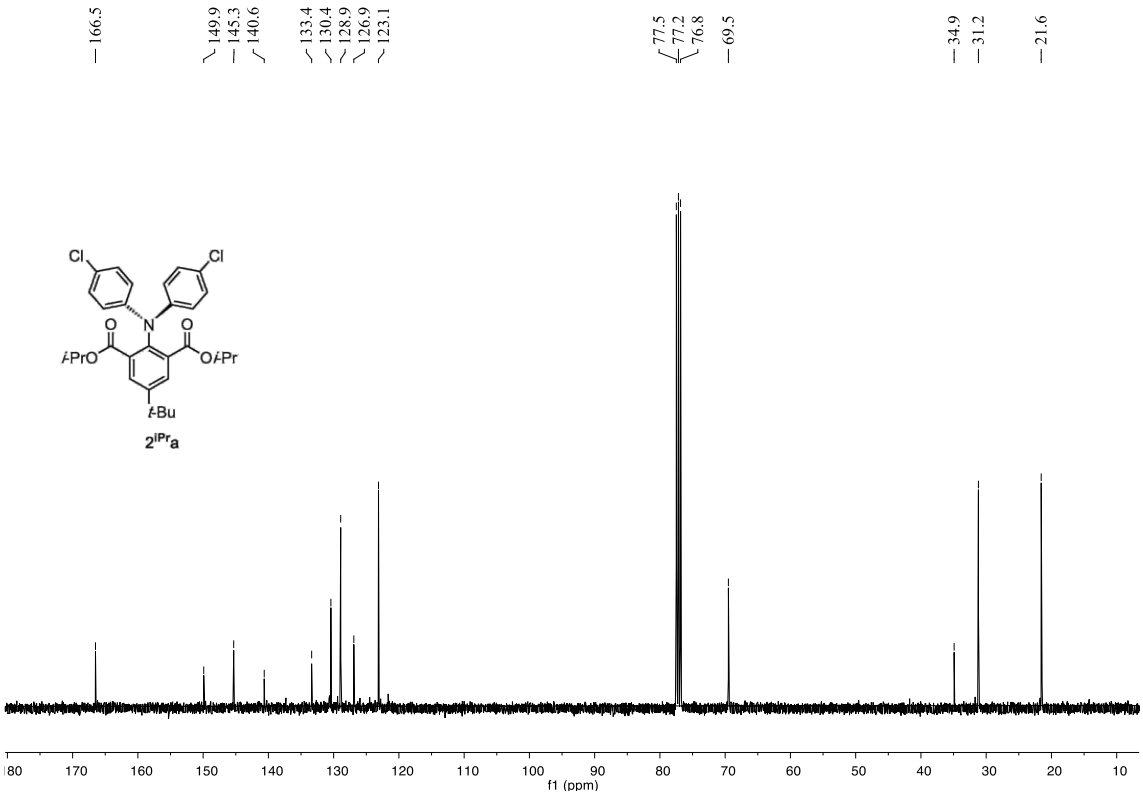

Diisopropyl 2-(bis(4-(trifluoromethyl) phenyl) amino)-5-(tert-butyl) isophthalate (2^{iPr}b)

^{1}H NMR (400 MHz, $CDCl_3$) δ (ppm) 7.80 (s, 2H), 7.44 (d, *J* = 8 Hz, 4H), 7.07 (d, *J* = 8 Hz, 4H), 4.85 (m, *J* = 24 Hz, 2H), 1.38 (s, 9H), 0.99 (d, *J* = 4 Hz, 12H).

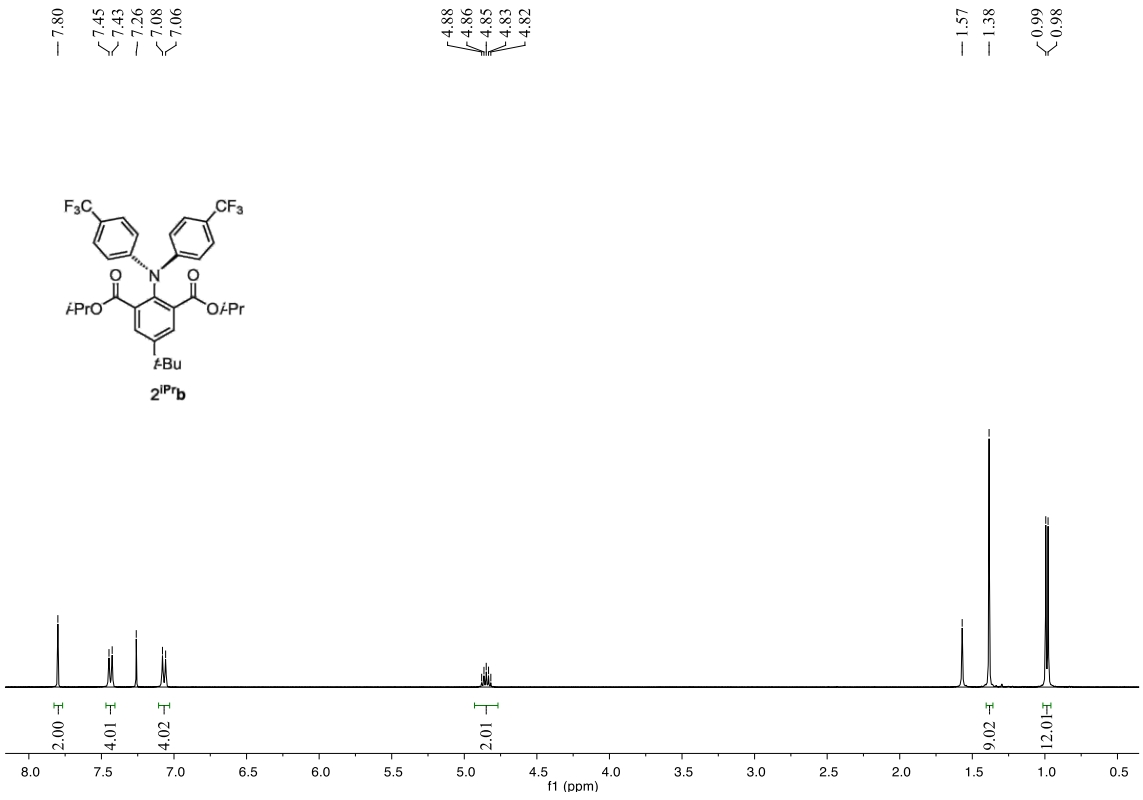

^{13}C NMR (100 MHz, $CDCl_3$) δ (ppm) 166.1, 150.9, 149.1, 140.1, 133.4, 130.7, 126.2 (q, $^{3}J_{C-F}$ = 10 Hz), 124.5 (q, $^{1}J_{C-F}$ = 270 Hz), 124.0 (q, $^{2}J_{C-F}$ = 30 Hz), 121.6, 69.7, 35.0, 31.2, 21.4.

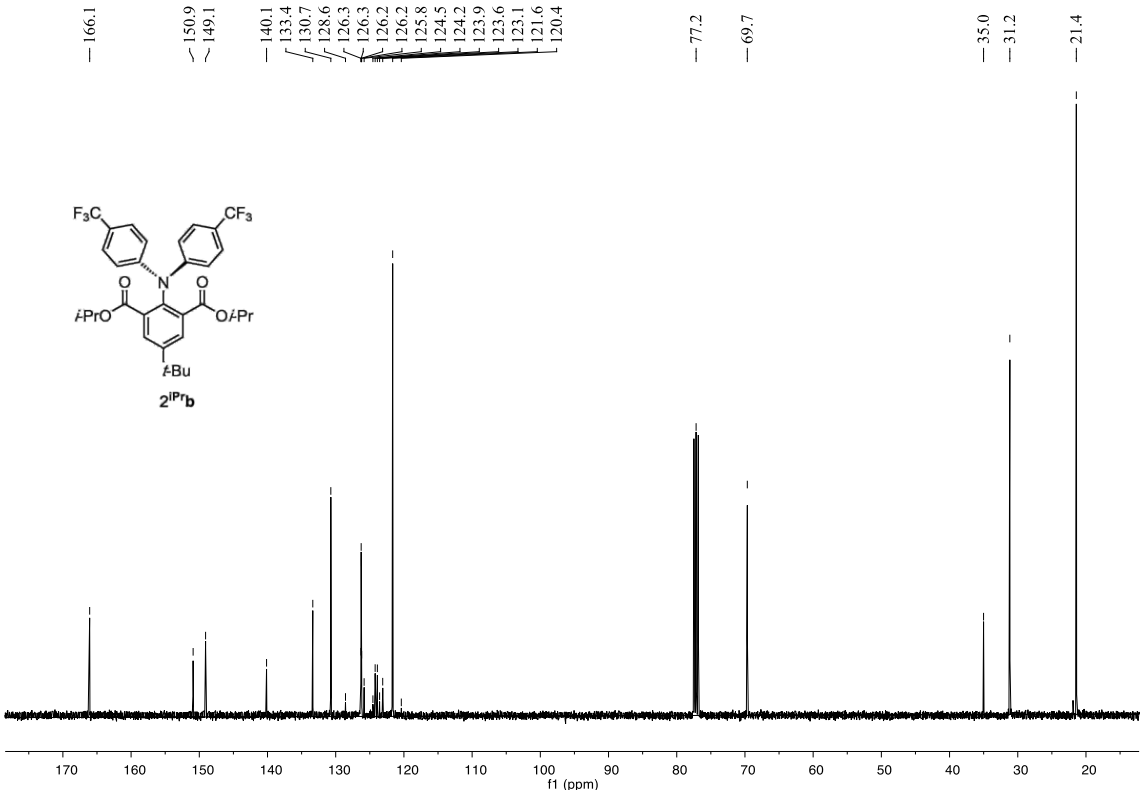

^{19}F NMR (376 MHz, $CDCl_3$) δ (ppm) -62.45.

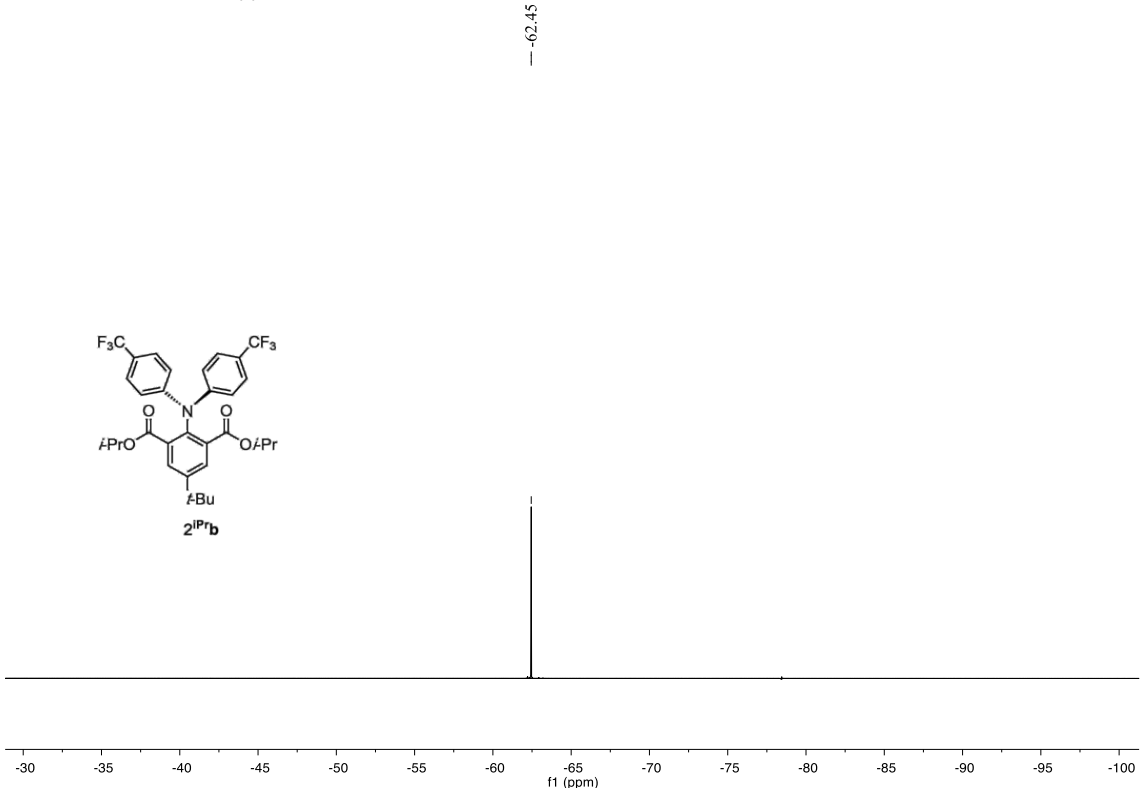

Dimethyl 2-(bis(4-methoxyphenyl)amino)-5-(tert-butyl) isophthalate ($2^{Me}c$)

^{1}H NMR (400 MHz, $CDCl_3$) δ 7.69 (s, 2H), 6.88 (d, *J* = 8.0 Hz, 4H), 6.74 (s, 4H), 3.74 (s, 6H), 3.50 (s, 6H), 1.33 (s, 9H).

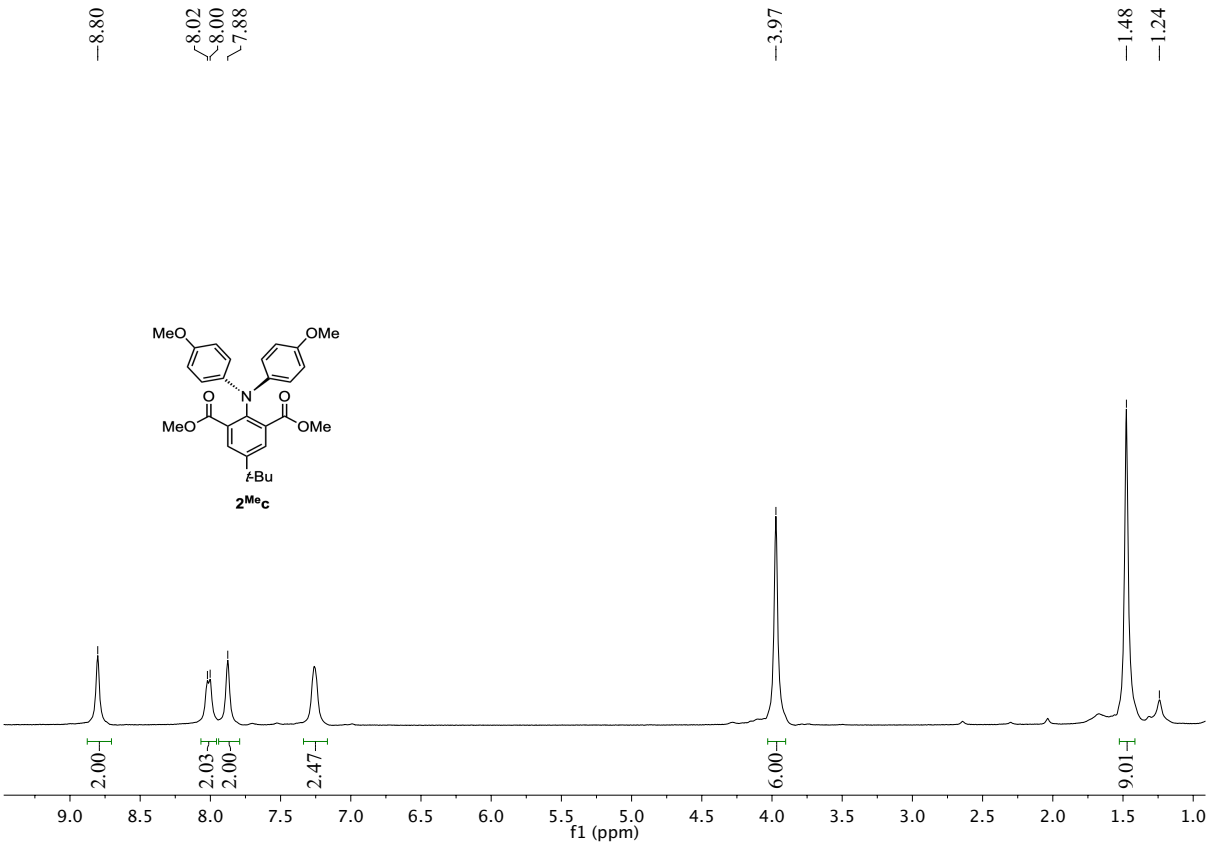

^{13}C NMR (100 MHz, $CDCl_3$) δ 168.5, 154.8, 147.7, 142.4, 141.3, 131.6, 130.8, 123.5, 114.2, 55.5, 52.2, 34.7, 31.2.

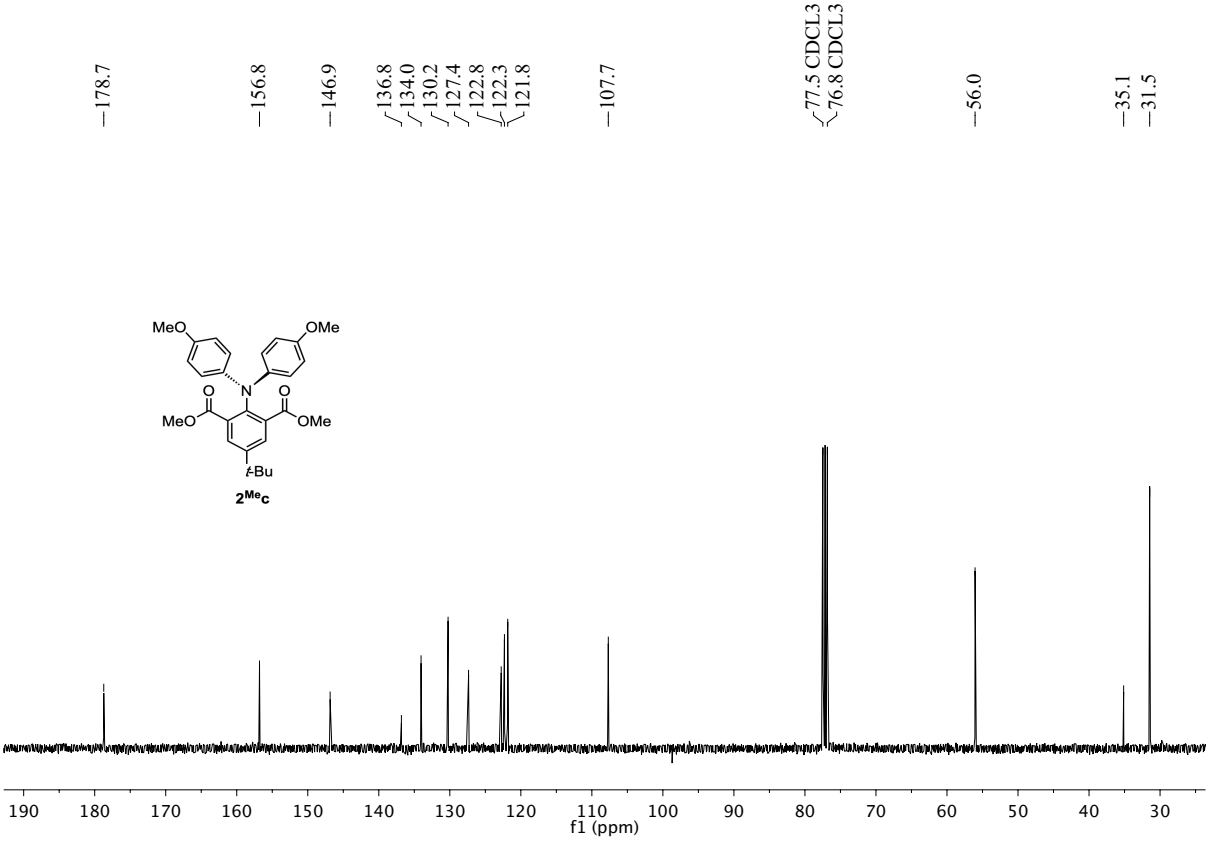

Reference

[1] G. M. Sheldrick, A short history of *SHELX. Acta Cryst*. **2008**, *A64*, 112–122.

[2] C. B. Hüebschle, G. M. Sheldrick, B. Dittrich, *ShelXle*: a Qt graphical user interface for *SHELXL*. *J. Appl. Cryst.* **2011**, *44*, 1281–1284.

[3] Persistence of Vision Raytracer (*ver*. 3.7.0); Persistence of Vision Pty. Ltd., 2016; Retrieved from http://www.povray.org/download/

[4] (a). F. Neese, The ORCA program system. *Wiley. Interdiscip. Rev. Comput. Mol. Sci.* **2012**, *2*, 73-78; (b) F. Neese, Software update: the ORCA program system, version 4.0. *Wiley. Interdiscip. Rev. Comput. Mol. Sci.* **2017**, *8*, e1327.

[5] E. D. Glendening, C. R. Landis, F. *Weinhold.* NBO 6.0: Natural bond orbital analysis program. *J. Comput. Chem.* **2013**, 34, 1429-1437.

[6] T. Lu, F. Chen, Multiwfn: A multifunctional wavefunction analyser. *J. Comput. Chem.* **2012**, *33*, 580-592.

[7] C. Riplinger, F. Neese, An efficient and near linear scaling pair natural orbital based local coupled cluster method. *J. Chem. Phys.* **2013**, *138*, 034106.